Article

Heteromeric channels formed by TRPC1, TRPC4 and TRPC5 define hippocampal synaptic transmission and working memory

Jenny Bröker-Lai[1], Astrid Kollewe[2,†], Barbara Schindeldecker[3,†], Jörg Pohle[1,4,†], Vivan Nguyen Chi[5,†], Ilka Mathar[1], Raul Guzman[3], Yvonne Schwarz[3], Alan Lai[1], Petra Weißgerber[6], Herbert Schwegler[7], Alexander Dietrich[8], Martin Both[5], Rolf Sprengel[9] (iD), Andreas Draguhn[5], Georg Köhr[4], Bernd Fakler[2,10], Veit Flockerzi[6], Dieter Bruns[3] & Marc Freichel[1,*] (iD)

Abstract

Canonical transient receptor potential (TRPC) channels influence various neuronal functions. Using quantitative high-resolution mass spectrometry, we demonstrate that TRPC1, TRPC4, and TRPC5 assemble into heteromultimers with each other, but not with other TRP family members in the mouse brain and hippocampus. In hippocampal neurons from _Trpc1/Trpc4/Trpc5_-triple-knockout (_Trpc1/4/5$^{-/-}$_) mice, lacking any TRPC1-, TRPC4-, or TRPC5-containing channels, action potential-triggered excitatory postsynaptic currents (EPSCs) were significantly reduced, whereas frequency, amplitude, and kinetics of quantal miniature EPSC signaling remained unchanged. Likewise, evoked postsynaptic responses in hippocampal slice recordings and transient potentiation after tetanic stimulation were decreased. _In vivo_, _Trpc1/4/5$^{-/-}$_ mice displayed impaired cross-frequency coupling in hippocampal networks and deficits in spatial working memory, while spatial reference memory was unaltered. _Trpc1/4/5$^{-/-}$_ animals also exhibited deficiencies in adapting to a new challenge in a relearning task. Our results indicate the contribution of heteromultimeric channels from TRPC1, TRPC4, and TRPC5 subunits to the regulation of mechanisms underlying spatial working memory and flexible relearning by facilitating proper synaptic transmission in hippocampal neurons.

Keywords cross-frequency coupling; hippocampal synaptic transmission; relearning; spatial working memory; TRPC1/C4/C5 heteromeric assembly

Introduction

The seven canonical transient receptor potential channels (TRPC1 to TRPC7) form non-selective cation channels that are activated in response to the stimulation of phospholipase C-coupled receptors, causing Na$^+$ and Ca^{2+} entry into the cell, thus leading to the depolarization of the membrane potential and the initiation of Ca^{2+}-dependent intracellular cascades. Based on structural homology, members of the TRPC subfamily can be divided into three subgroups: TRPC1/TRPC4/TRPC5, TRPC3/TRPC6/TRPC7, and TRPC2 (Montell _et al_, 2002; Wu _et al_, 2010). In mice, the _Trpc1_, _Trpc4_, and _Trpc5_ genes are expressed together in several subregions of the hippocampus, as demonstrated by _in situ_ hybridization and immunohistochemistry (Strübing _et al_, 2001; Freichel _et al_, 2005; Fowler _et al_, 2007). They co-localize in the stratum pyramidale of the hippocampal CA1-CA3 regions and the granule layer of the dentate gyrus; weaker expression is found in the hilus and the ventral subiculum.

In heterologous co-expression experiments, TRPC1, TRPC4, and TRPC5 were shown to interact with each other, but not with members of the TRPC3/TRPC6/TRPC7 subgroup (Hofmann _et al_,

1 Institute of Pharmacology, Heidelberg University, Heidelberg, Germany
2 Institute of Physiology, University of Freiburg, Freiburg, Germany
3 Center for Integrative Physiology and Molecular Medicine, Saarland University, Homburg, Germany
4 Physiology of Neural Networks, Psychiatry/Psychopharmacology, Central Institute of Mental Health, J5, Heidelberg University, Mannheim, Germany
5 Institute of Physiology and Pathophysiology, Heidelberg University, Heidelberg, Germany
6 Experimental and Clinical Pharmacology and Toxicology, Saarland University, Homburg, Germany
7 Institute of Anatomy, University of Magdeburg, Magdeburg, Germany
8 Walther-Straub-Institute for Pharmacology and Toxicology, Ludwig-Maximilians-University München, München, Germany
9 Max Planck Research Group of the Max Planck Institute for Medical Research at the Institute for Anatomy and Cell Biology, Heidelberg University, Heidelberg, Germany
10 BIOSS, Center for Biological Signaling Studies, University of Freiburg, Freiburg, Germany‡
   *Corresponding author. Tel: +49 6221 54 86861; E-mail: marc.freichel@pharma.uni-heidelberg.de
   †These authors contributed equally to this work
   ‡Correction added on 15 September 2017 after first online publication: Affiliation 10 was added

2002). Other reports described heterologous interactions of TRPC1 with all members of the TRPC subfamily (Storch *et al*, 2012) as well as with TRPV4 and TRPP2 (Ma *et al*, 2011; Du *et al*, 2014). Moreover, co-immunoprecipitations from brain membrane fractions suggested the formation of heteromultimers between TRPC1, TRPC4, and TRPC5 (Goel *et al*, 2002; Hofmann *et al*, 2002), as well as with TRPC3 and TRPC6 (Strübing *et al*, 2003) in embryonic brain. However, these observations are obscured by the lack of subtype-specific antibodies and rigorous negative controls as provided by the respective target-knockout mice.

While TRPC channels have been implicated in a variety of neuronal functions, including neuronal excitability (Faber *et al*, 2006; Stroh *et al*, 2012; Phelan *et al*, 2013), excitotoxicity (Phelan *et al*, 2012, 2013), neurogenesis (Li *et al*, 2012), and neurite outgrowth (Greka *et al*, 2003; Li *et al*, 2005; Hui *et al*, 2006), the role of TRPC1-, TRPC4-, and TRPC5-containing channels in synaptic transmission and neurotransmitter release remains sparse (Hartmann *et al*, 2008; Riccio *et al*, 2009; Shen *et al*, 2013). TRPC1 was identified as a mGluR1-evoked slow EPSC channel in cerebellar Purkinje cells based on interference with an anti-TRPC1 antibody (Kim *et al*, 2003). However, subsequent experiments with several TRPC-deficient mouse models revealed TRPC3 as a mGluR1-evoked slow EPSC channel (Hartmann *et al*, 2008). In infantile $Trpc5^{-/-}$ mice, synaptic strength was diminished at inputs to the amygdala, but it was not significantly altered in older $Trpc5^{-/-}$ mice (Riccio *et al*, 2009). In the olfactory bulb, measurements of inhibitory postsynaptic currents (IPSCs) in mitral/tufted cells demonstrated a reduction in GABA release from granule cells in $Trpc1/Trpc4^{-/-}$-double-knockout mice (Stroh *et al*, 2012). On the organismal level, $Trpc4^{-/-}$ and $Trpc5^{-/-}$ mice exhibit a reduced anxiety-like phenotype, when presented with stimuli triggering innate fear responses (Riccio *et al*, 2009, 2014). Both TRPC4 and TRPC5 are causally involved in epileptogenesis, as well as in associated seizures and early death in mice (Phelan *et al*, 2012, 2013). Additionally, in a mouse model for Huntington's disease (HD), an involvement of TRPC5 activation via S-glutathionylation of Cys176/178 was reported in the pathogenesis of HD (Hong *et al*, 2015).

The hippocampus is postulated as storage region for the spatial map, and the formation of the spatial map was shown to depend on the NMDA receptor-induced plasticity of hippocampal CA3 to CA1 synapses (Morris *et al*, 1986a,b; Bannerman *et al*, 1995, 2012; Tsien *et al*, 1996a,b). This hypothesis was recently experimentally challenged by the finding of Bannerman *et al* that the NMDA receptors at dorsal CA3 to CA1 synapses are not necessary for the formation of spatial maps but for decision making (Bannerman *et al*, 2012).

The function of the TRPC1/TRPC4/TRPC5 subfamily for memory formation and synaptic plasticity in the hippocampus has been largely unknown. Here, we demonstrate the specific formation of heteromultimers from TRPC1, TRPC4, and TRPC5 in the mouse brain and hippocampus, using knockout-controlled affinity purifications together with quantitative high-resolution mass spectrometry analysis. The combined deletion of *Trpc1*, *Trpc4*, and *Trpc5* in mice uncovered a role for TRPC1/4/5 channels in neuronal communication and hippocampal function. In the absence of TRPC1/4/5, the action potential-evoked EPSC amplitude was markedly reduced in autaptic hippocampal neurons, while synapse density and miniature EPSC (mEPSC) frequency in neuronal mass cultures remained unchanged. In the same line, synaptic transmission was also reduced in hippocampal slice recordings.

These cellular peculiarities were accompanied by impaired cross-frequency phase–amplitude coupling of theta and gamma oscillations in hippocampal networks, as well as by severe deficits in both spatial working memory (SWM) and flexible spatial relearning as demonstrated in independent hippocampus-specific tasks, while spatial reference memory (SRM) was not affected. These behavioral deficits were not associated with changes in brain morphology.

Overall, our results suggest that heteromultimeric channels composed of TRPC1, TRPC4, and TRPC5 subunits contribute to the regulation of the mechanisms underlying working memory and flexible relearning by facilitating proper synaptic transmission in hippocampal neurons.

Results

TRPC1, TRPC4, and TRPC5 proteins co-assemble into heterotetrameric channels in the mouse brain and hippocampus

To test the assembly of TRPC1, TRPC4, and TRPC5, we combined quantitative high-resolution mass spectrometry with affinity purifications (APs) using isoform-specific antibodies (see Materials and Methods) on membrane fractions prepared from wild-type and target-knockout brains. Evaluation of these APs demonstrated the robust co-assembly of all three TRPC isoforms in both whole brain and hippocampus (Figs 1 and EV1). Thus, TRPC4 and TRPC5 were effectively co-purified in APs with an anti-TRPC1 antibody from wild-type membranes, but not from TRPC1-knockout material (left part, Fig 1). Similarly, the anti-TRPC4 antibody specifically and abundantly co-purified TRPC1 and TRPC5, and the anti-TRPC5 antibody co-purified TRPC1 and TRPC4 proteins (middle and right parts, Fig 1). In contrast, mass spectrometry did not detect other members of the TRPC family, nor any other TRP protein in any of the AP eluates analyzed. These results indicate the formation of heteromultimeric channels from TRPC1, TRPC4, and TRPC5 subunits, although the exact stoichiometry of such assemblies cannot be derived.

TRPC1/4/5 channels regulate action potential-evoked transmitter release

The physiological role of TRPC1/4/5 channels in synaptic transmission was analyzed in autaptic hippocampal neuron cultures. Short stimulation of these neurons in the voltage-clamp mode evoked single action potentials that triggered a robust synaptic response mediated by AMPA receptors (Guzman *et al*, 2010). Compared to control cells, TRPC1/4/5-triple-deficient neurons displayed a significant reduction in amplitude and charge of the EPSCs (Fig 2A and B). In contrast, TRPC1/4/5 deficiency affected neither mEPSC frequency, amplitude, nor the time course of quantal signaling (Fig 2C and D), indicating that the properties of postsynaptic signal generation and transmitter sensing are unchanged in the absence of TRPC1, TRPC4, and TRPC5 proteins. To investigate whether deficits in synaptic transmission are accompanied by alterations in synapse density, mass cultures of hippocampal neurons were stained with antibodies against the vesicular marker protein synaptophysin. No changes in the number or area of synapses were observed (Fig 2E and F). Taken together, TRPC1/4/5 channels in hippocampal
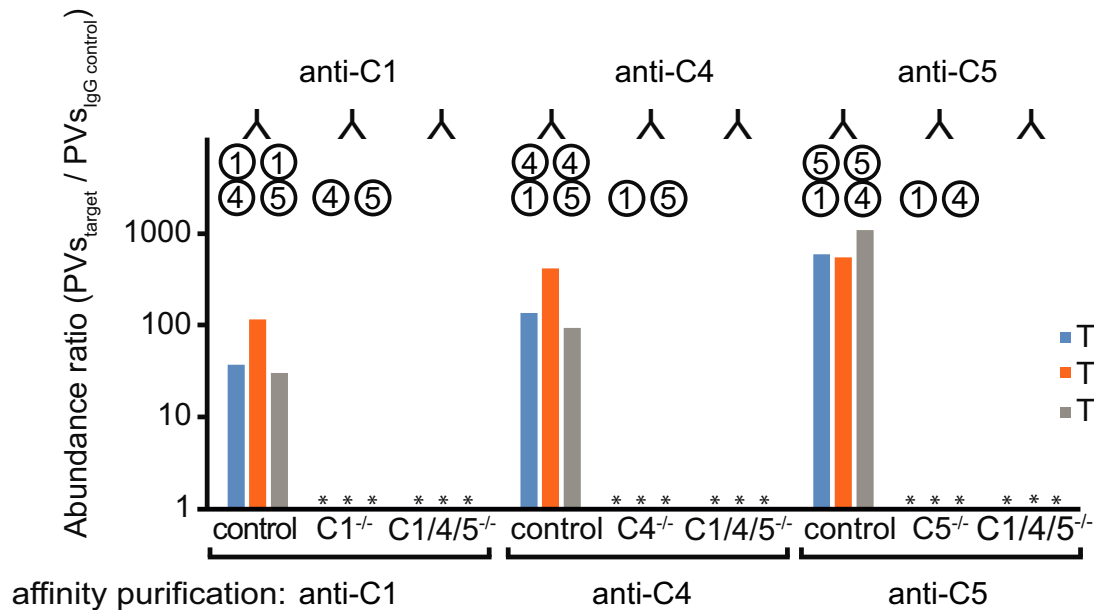
Figure 1. Heteromultimer formation between TRPC1, TRPC4, and TRPC5.

Abundance ratios (see Materials and Methods) determined for TRPC1, TRPC4, and TRPC5 in affinity purifications with antibodies specifically targeting TRPC1 (anti-C1), TRPC4 (anti-C4), and TRPC5 (anti-C5) proteins, in membrane fractions prepared from brains of wild-type control, $Trpc1^{-/-}$, $Trpc4^{-/-}$, $Trpc5^{-/-}$, or $Trpc1/4/5^{-/-}$ animals ($Trpc1^{-/-}$, $Trpc4^{-/-}$, or $Trpc5^{-/-}$ labeled as C1$^{-/-}$, C4$^{-/-}$, or C5$^{-/-}$, and $Trpc1/4/5^{-/-}$ labeled as C1/4/5$^{-/-}$). Asterisks denote lack of protein-specific peptides in the respective affinity purifications. Inset depicts possible subunit assemblies for the respective affinity purifications.

neurons facilitate evoked transmitter release potentially by altering neuronal excitability or presynaptic Ca^{2+} dynamics.

Deletion of the *Trpc1*, *Trpc4*, and *Trpc5* genes does not cause morphological changes in the brain

To test whether the deletion of *Trpc1*, *Trpc4*, and *Trpc5* affects the cellular integrity of the hippocampus, we compared the hippocampal structures by immunohistological and histochemical stainings of brain slices from adult $Trpc1/4/5^{-/-}$ and control mice. Immunostainings using anti-GluA1 antibodies (Fig 3A) showed the typical expression pattern of the α-amino-3-hydroxy-5-methyl-4-isoxazolepropionic (AMPA) receptor subunit GluA1 (Zamanillo *et al*, 1999; Jensen *et al*, 2003). Similar to control mice, strong GluA1 immunostaining was detected in the stratum radiatum, the stratum oriens, and the molecular layer of the dentate gyrus (DG) in the hippocampus of $Trpc1/4/5^{-/-}$ animals. In both control and $Trpc1/4/5^{-/-}$ mice, the GluA1 expression was highest in the CA1 and lowest in the stratum pyramidale (Fig 3A), suggesting a regular dendritic enrichment of AMPA receptors in both CA1, CA2, CA3 pyramidal and DG granule cells. Anti-GFAP stainings revealed that the manually determined number and the distribution of GFAP-positive astrocytes in the hippocampal slices were comparable between control and $Trpc1/4/5^{-/-}$ mice (Fig 3B). Similarly, the number and distribution of somatostatin-positive interneurons, both in the stratum oriens and in the hilus region of the DG, were unchanged (Fig 3C). The histological analysis by Nissl staining of horizontal brain sections showed no obvious differences in the thickness of the CA1, CA3, and the outer DG granule cell layers between the dorsal hippocampus of control and $Trpc1/4/5^{-/-}$ mice,

respectively (Fig 3D). In conclusion, the loss of TRPC1, TRPC4, and TRPC5 was not associated with any major alterations in the brain morphology or the thickness of the cortical layer as evaluated by anti-NeuN staining of coronal sections (Fig 3E).

Unchanged basal neuronal network oscillations with impaired cross-frequency phase–amplitude coupling in $Trpc1/4/5^{-/-}$ mice

Next, we checked whether electrical activity in hippocampal networks of $Trpc1/4/5^{-/-}$ mice was impaired. Freely moving animals were recorded in 5-h sessions according to the experimental setup depicted in Fig 4A. The frequency distributions displayed typical activity-dependent features as previously described (Tort *et al*, 2008; Scheffzuk *et al*, 2013). In summary, frequency peaks for theta and gamma oscillations during REM sleep were not altered (Fig 4B). Frequency peaks and power for both theta and gamma oscillations during REM sleep were unchanged (Fig 4B, C and F). We further analyzed how gamma amplitude was modulated by the theta phase. General appearance of cross-frequency couplings was similar to previous findings (Scheffer-Teixeira *et al*, 2012) with a modulation of low gamma (50–80 Hz) during REM sleep (Fig 4D). Indeed, gamma oscillations in TRPC1/4/5-deficient animals were broadly distributed along theta-phase cycles (Fig 4E), whereas control animals showed the typical "waning" and "waxing" features as described in earlier studies (Chrobak & Buzsaki, 1998). This suggests a desynchronization between gamma oscillations and theta phase. Consistently, the modulation index of cross-frequency phase–amplitude coupling for low gamma was significantly reduced in $Trpc1/4/5^{-/-}$ animals, compared to the controls (Fig 4G). Taken together, the deletion of TRPC1/4/5
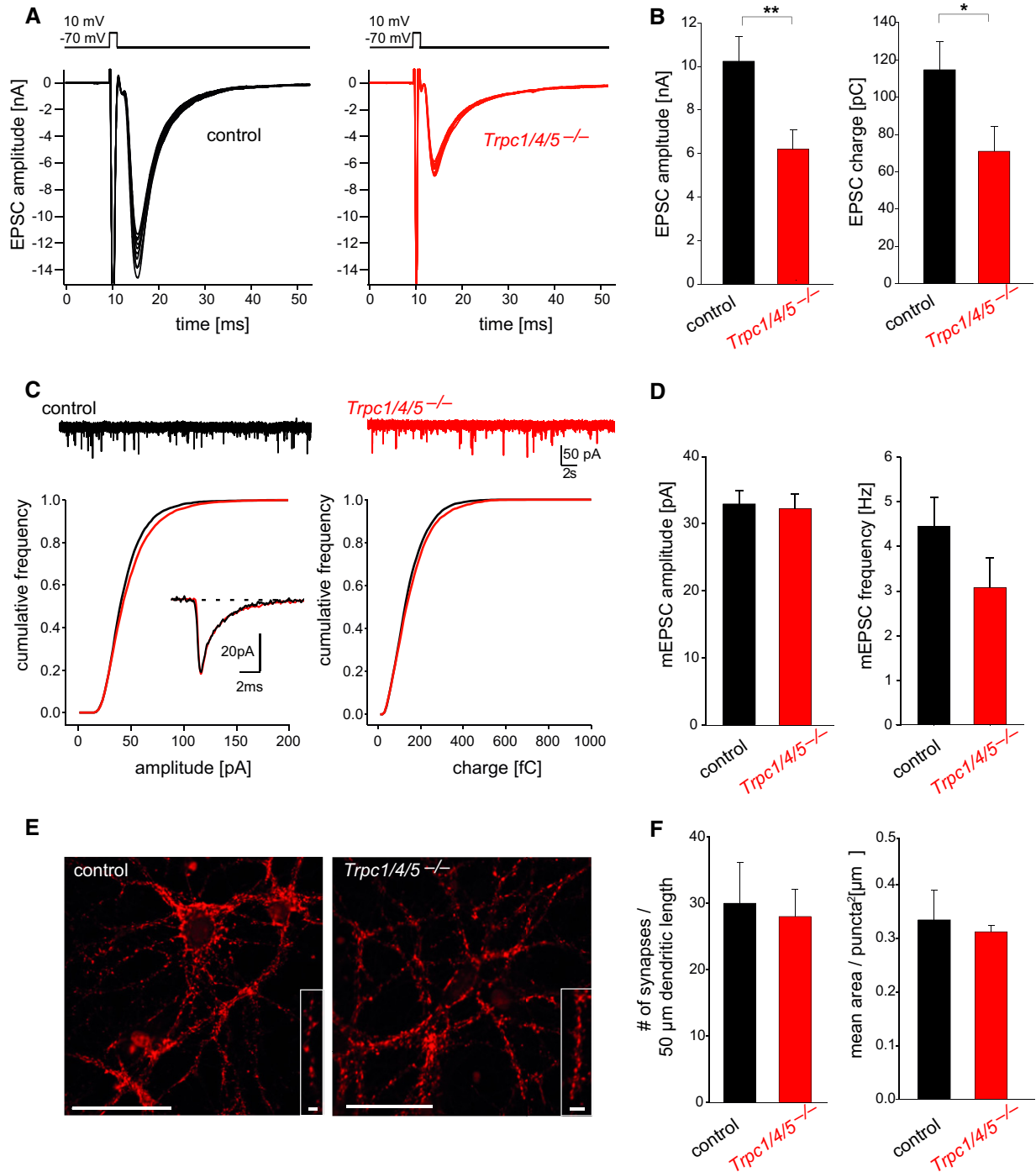
Figure 2.   Impaired action potential-evoked transmitter release in TRPC1/4/5-deficient hippocampal neurons.

A   Exemplary recordings of evoked EPSCs from autaptic hippocampal neurons.

B   Summary plots for EPSC parameters. The loss of TRPC1, TRPC4, and TRPC5 reduces the amplitude (**P = 0.0058) and charge of EPSCs (*P = 0.032) (n = 63 for $Trpc1/4/5^{-/-}$, n = 66 for controls). Statistical significance was determined using two-tailed unpaired Student's t-test.

C, D   (C) Exemplary recordings of mEPSCs from neurons in mass culture. The cumulative frequency distribution of mEPSC amplitude and charge, as well as the quantitative analyses of both frequency and amplitude (D), shows that TRPC1/4/5 deficiency does not alter the properties of quantal signaling (n = 14 for $Trpc1/4/5^{-/-}$, n = 20 for controls).

E   Representative epifluorescence images of neurons immunolabeled with synaptophysin. Scale bar (inset), 5 μm.

F   The loss of TRPC channels does not alter the density of synapses determined per 50 μm length of neuronal processes or their respective size (n = 17 for $Trpc1/4/5^{-/-}$, n = 15 for controls).

Data information: Results are shown as mean ± SEM.

impairs the interaction between low- and high-frequency hippocampal network oscillations.

Synaptic transmission and firing output are reduced in hippocampal area CA1 of *Trpc1/4/5*[−/−] mice without changing synaptic long-term potentiation (LTP) or depotentiation

In acute hippocampal slices of adult animals, we analyzed the plasticity of CA3-to-CA1 synapses. Upon stimulation of Schaffer collateral CA3 axons ("1" in Fig 5A), comparable axonal spiking of CA3 neurons was obtained (Fig 5B), both in control and in *Trpc1/4/5*[−/−] mice. Postsynaptic currents, measured as local field potentials (LFPs) (Fig 5C), in stratum radiatum ("2" in Fig 5A) as well as the postsynaptic firing of CA1 cells, measured in stratum pyramidale ("3" in Fig 5A) as population spikes (Fig 5D), were reduced in slices from *Trpc1/4/5*[−/−] mice. Hence, in order to assure comparable baseline LFPs for plasticity experiments below (Fig 5I–K), baseline stimulation intensity was adjusted to higher levels in TRPC1/4/5-deficient slices (Fig 5E). Equal LFPs elicited comparable firing of the postsynaptic CA1 cells (Fig 5F and G). A left shift ("E-S-potentiation") at the second pulse of a 50-ms paired pulse was observed in both control (Fig 5F) and *Trpc1/4/5*[−/−] slices (Fig 5G), indicating no prominent inhibition on the second pulse under our experimental conditions. When activating the same number of presynaptic fibers (compare Fig 5B), LFP paired-pulse ratios were increased in *Trpc1/4/5*[−/−] mice (Fig 5H, main), pointing to altered short-term facilitation. Yet, LFP paired-pulse ratios versus the respective first LFP slopes of the paired pulses (Fig 5H, inset) were found to be similar for *Trpc1/4/5*[−/−] mice and controls, suggesting an unchanged synaptic release probability in *Trpc1/4/5*[−/−] mice. The transient potentiation after 100-Hz stimulation was impaired in *Trpc1/4/5*[−/−] acute hippocampal slices (Fig 5I), further suggesting altered short-term plasticity in *Trpc1/4/5*[−/−] animals. Since memory function, among others, relies on synaptic plasticity, we studied different aspects of long-term plasticity similar to Nicholls *et al* (2008) including a modified NMDAR-dependent (Fig 5K, arrow 2) and NMDAR-independent (arrow 3) depotentiation protocol (Kemp *et al*, 2000). With these protocols, we did not reveal any impairment neither in long-term potentiation (Fig 5J) nor in successful depotentiation (Fig 5K) in the absence of the three TRPC channel subunits TRPC1, TRPC4, and TRPC5.

Deletion of the *Trpc1*, *Trpc4*, and *Trpc5* genes impairs spatial working memory and relearning competence

Changes in synaptic transmission are frequently associated with differences in hippocampus-dependent memory formation or consolidation (Tsien *et al*, 1996b; Fuchs *et al*, 2007; Du *et al*, 2008; Brigman *et al*, 2010). For characterization of the potential alterations in general behavioral patterns of *Trpc1/4/5*[−/−] mice, we tested elementary behavioral skills using a SHIRPA protocol (Filali & Lalonde, 2016; Zhang *et al*, 2016). No differences in spontaneous behavior and activity, reflexes, visual, or hearing skills were observed. The analysis of a rotarod test revealed no alterations in motor skills. Taken together, these results indicate that there are no major deficits that could impact the animals' performance in the subsequent learning and memory tasks.

Hippocampus-dependent behavior was analyzed using well-established paradigms of the T-maze, Morris water maze, and radial maze. In the T-maze test, mice usually prefer to seek a food pellet in a novel arm and therefore need to recall the previously visited test arm. Hence, working memory is assessed in this paradigm (Wenk, 2001; Jang *et al*, 2013). The time course of error counts, and more clearly the slopes of their log best fits, illustrates that the control mice learned to alternate their choice of visited arms as the T-maze test progressed. Already from the fifth training day on, they reached an error rate of merely 20%. In contrast, *Trpc1/4/5*[−/−] animals consistently performed hardly below the random chance level, indicating impairment in spontaneous alternation and thus in spatial working memory (SWM) (Fig 6A). A comparison of the overall change in performances over time between the two groups confirms the impaired performance of mutant mice observed on individual test days.

To corroborate deficits in SWM for the triple-deficient animals, we performed a radial maze test, where re-entries into previously visited (empty) arms are regarded as SWM errors (Schmitt *et al*, 2005; Bannerman *et al*, 2008; Penley *et al*, 2013). Also in this experiment, the number of errors was significantly increased in *Trpc1/4/5*[−/−] mice on the majority of days during the early test phase (Fig 6B), emphasizing impaired SWM in TRPC1/4/5-deficient mice compared to controls.

Spatial reference memory (SRM) was assessed using a standard protocol of the Morris water maze (Fig 7A), in which mice were

---

Figure 3. Inactivation of the *Trpc1*, *Trpc4*, and *Trpc5* genes does not affect the overall anatomical structure and the cellular distribution of the mouse brain.

A–C   Immunohistology of coronal brain sections illustrates comparable patterns of GluA1 (A), GFAP (B), and somatostatin (C) expression in *Trpc1/4/5*[−/−] and control mice. (B) The number of glial cells (mean ± SEM) is as follows (*Trpc1/4/5*[−/−] versus controls): in CA1: subgranular zone: 69.00 ± 6.66 versus 70.67 ± 6.23 (P = 0.8638), Str. molekulare: 110.00 ± 15.63 versus 89.00 ± 6.08 (P = 0.2788), Str. lacunosum: 100.33 ± 9.91 versus 109.67 ± 6.12 (P = 0.4677), Str. radiatum: 121.00 ± 16.29 versus 118.00 ± 12.66 (P = 0.8914), Str. pyramidale: 52.67 ± 3.18 versus 53.00 ± 5.51 (P = 0.9607), Str. oriens: 90.67 ± 2.19 versus 88.00 ± 5.57 (P = 0.6788); in the cortex sector (1.2 × 1.7 mm): 109.00 ± 17.78 versus 128.33 ± 4.26 (P = 0.3498); the right cerebral hemispheres of three mice per genotype were analyzed. (C) The number of somatostatin-positive interneurons (mean ± SEM) is (*Trpc1/4/5*[−/−] versus controls): CA1: 100.50 ± 9.28 versus 78.33 ± 15.21 (P = 0.2419), CA2: 14.33 ± 0.99 versus 15.67 ± 1.71 (P = 0.5143), CA3: 65.17 ± 8.31 versus 52.17 ± 6.94 (P = 0.2577), hilus: 37.00 ± 3.16 versus 34.50 ± 2.63 (P = 0.5569); both cerebral hemispheres of three mice per genotype were analyzed.

D   Nissl staining of horizontal sections does not reveal any obvious changes in neuronal patterns of mutant and control mice. The thickness of the somata containing cell layer (μm; mean ± SEM) is (*Trpc1/4/5*[−/−] versus controls): CA1: 29.33 ± 1.63 versus 32.14 ± 2.41 (P = 0.3449), CA3: 49.58 ± 4.99 versus 48.83 ± 3.70 (P = 0.9039), outer DG: 23.79 ± 0.85 versus 21.75 ± 1.21 (P = 0.1819); in two independent tissue slices, both cerebral hemispheres were analyzed in three mice per genotype.

E   The thickness of the cortex layer in anti-NeuN immunostainings was comparable in control and *Trpc1/4/5*[−/−] mice (μm; mean ± SEM): 843.95 ± 17.05 versus 859.20 ± 42.87 (P = 0.7313); both cerebral hemispheres of three mice per genotype were analyzed.

Data information: Statistical significance was determined using two-tailed unpaired Student's *t*-test. Scale bars, 400 μm. CA1, cornus ammonis region 1; CA3, cornus ammonis region 3; CPu, caudate putamen; DG, dentate gyrus.
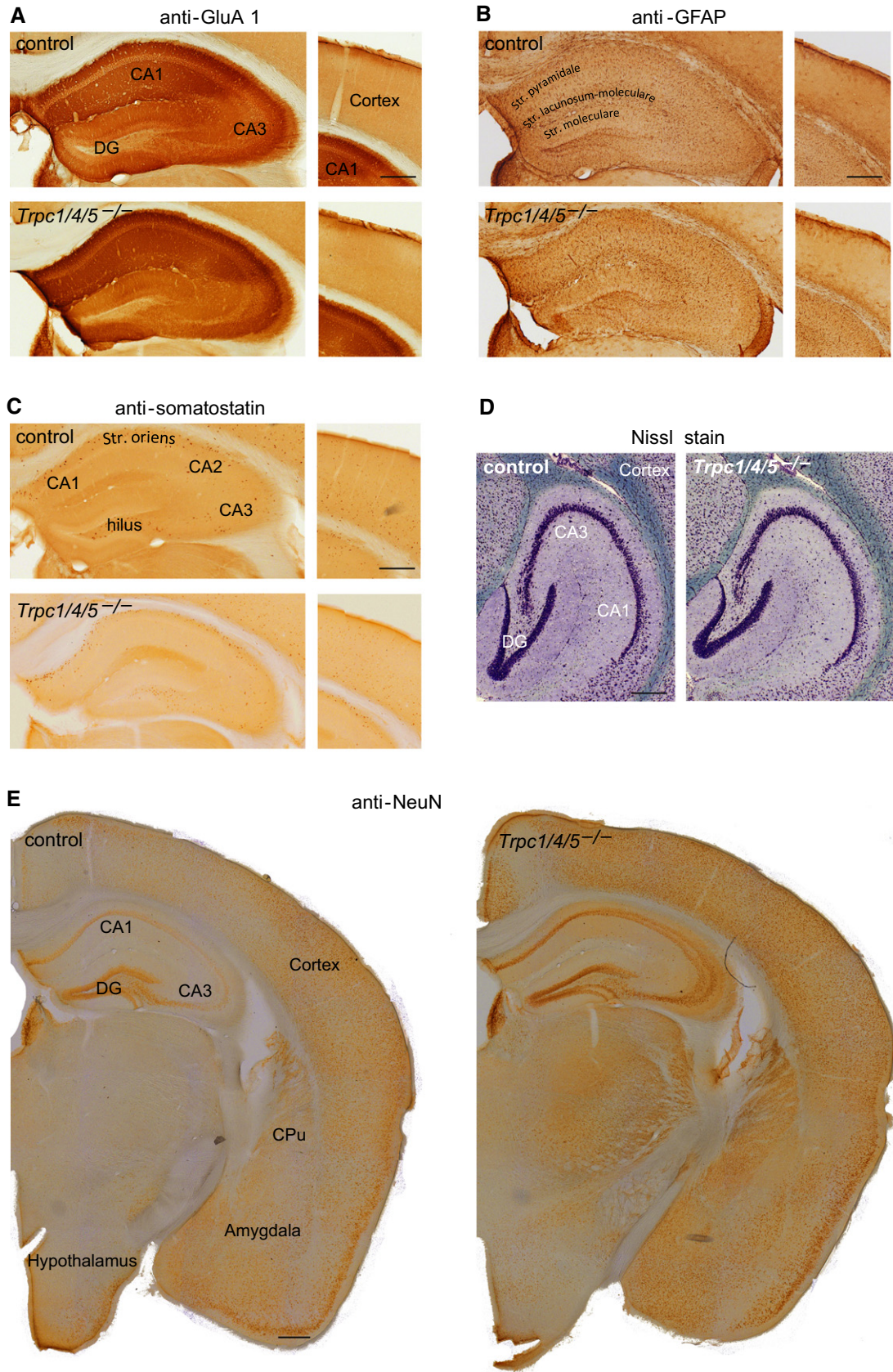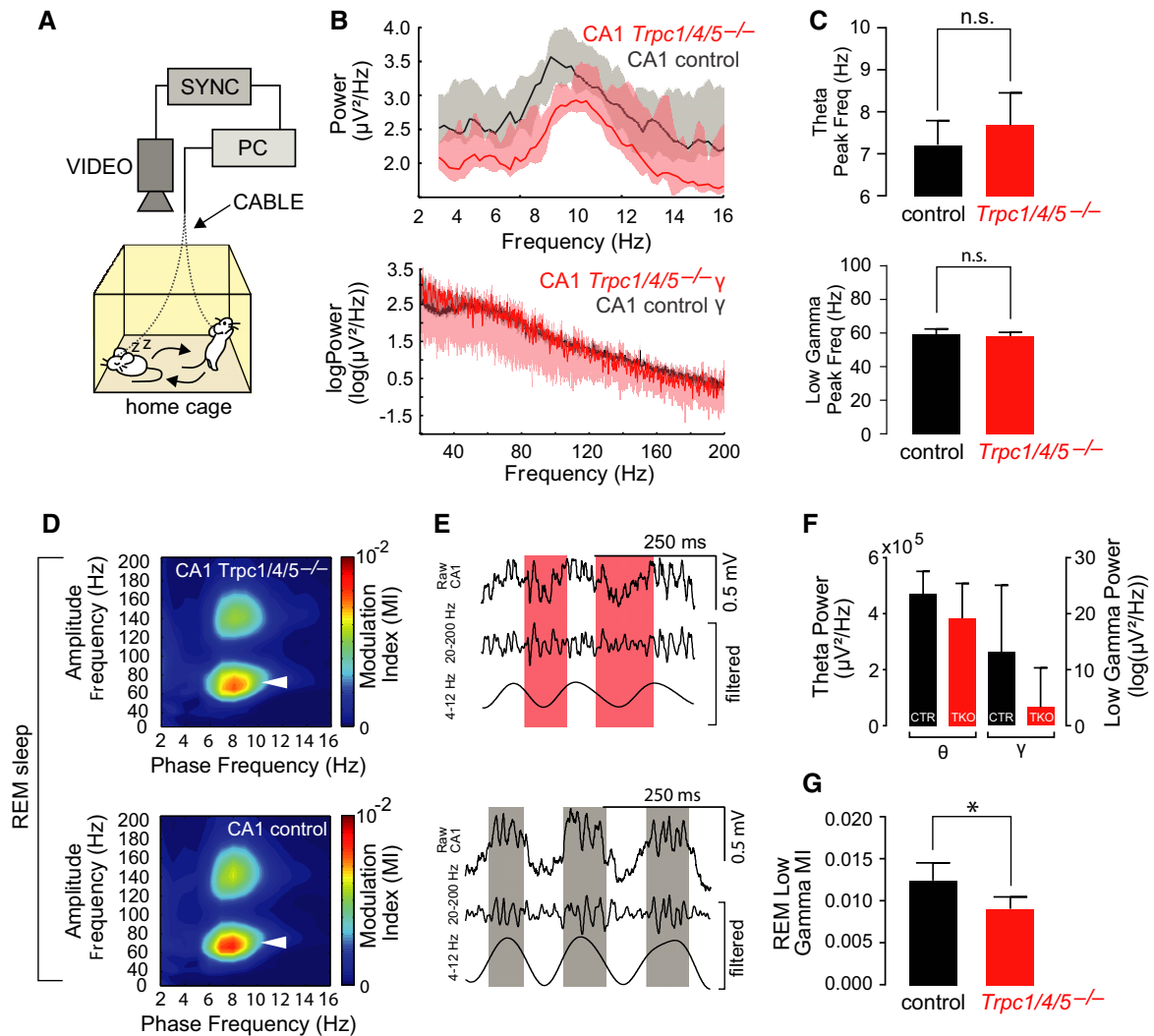
Figure 3.

Figure 4. Hippocampal network activity during rapid eye movement (REM) sleep is altered in *Trpc1/4/5*^{−/−} mice.

A   Scheme of experimental recording setup where video inputs (VIDEO) are synchronized (SYNC) to recorded local field potentials (LFPs) to the computer (PC).
B   Theta and gamma frequencies are not different between groups. Curves shown as median and 25th and 75th percentiles ($n = 5$ for *Trpc1/4/5*[−/−], $n = 5$ for controls).
C   Peak frequencies for theta and gamma oscillations are not significantly different from each other for both groups ($n = 5$ for *Trpc1/4/5*[−/−], $n = 5$ for controls).
D   Cross-frequency coupling during REM sleep shows reduced modulation of theta and low gamma for *Trpc1/4/5*[−/−] mice compared to controls (white arrows).
E   Raw LFPs and filtered LFPs for theta and gamma show diffuse distribution of gamma on theta oscillations for *Trpc1/4/5*[−/−] mice (red shades) when compared to controls, where gamma is superimposed mainly on the peak of theta cycles (gray shades) with the typical waning/waxing appearance.
F   Theta and low gamma power is not significantly different between control ($n = 5$) and *Trpc1/4/5*[−/−] mice ($n = 5$).
G   Modulation index (MI) for low gamma during REM sleep is reduced in *Trpc1/4/5*[−/−] ($n = 5$; *$P = 0.0179$) when compared to controls ($n = 5$; *$P = 0.0179$). CTR, control; TKO, *Trpc1/4/5*[−/−].

Data information: Results are shown as mean ± SEM. Statistical significance in (C and G) was determined using two-tailed unpaired Student's *t*-test.

trained to locate a hidden platform by using distant visual cues (Malleret *et al*, 1999). Latency and cumulative distance to reach the platform were measured. During the training phase, both parameters declined similarly in control and in *Trpc1/4/5*[−/−] mice (Fig 7B and C). Furthermore, after removing the platform on a subsequent probe trial (day 12), both genotypes showed similar preference for the training quadrant during their search, suggesting that all mice retained the location of the platform equally well (Fig 7D). Taken together, these findings indicate unchanged SRM in *Trpc1/4/5*[−/−] animals.

In the T-maze task (Fig 6A), the position of the first reward changes between trials, and hence, an adequate performance in this paradigm, requires behavioral flexibility (Nicholls *et al*, 2008; Kim *et al*, 2011). To investigate this behavioral quality in more detail, we applied a modified paradigm of the Morris water maze (Garthe *et al*, 2009) in a naive cohort of *Trpc1/4/5*[−/−] animals. To this end, a shortened training phase (days 1–3) with variable starting positions on each day was followed by a reversal part, in which the platform was relocated from the upper left to the lower right quadrant on day 4 to address relearning of a new goal

Figure 5. *Trpc1/4/5⁻/⁻* mice exhibit impaired synaptic transmission and firing output with unaltered long-term potentiation as well as depotentiation in hippocampal slice recordings.

A   (Left) Stimulation of Schaffer collaterals (CA3 axons). Recording electrodes (1) in stratum radiatum (2) and stratum pyramidale (3). (Right) Example traces of recording in stratum radiatum (top) and at the same time in stratum pyramidale (bottom).

B   Fiber volley in stratum radiatum as a measure for presynaptic axonal spiking versus stimulation intensity ($n = 21$ (11 mice) for $Trpc1/4/5^{-/-}$, $n = 15$ (9 mice) for controls; $P = 0.3427$, two-way ANCOVA of type II).

C   Input–output curve of LFPs versus stimulation intensity. No significant differences between control and $Trpc1/4/5^{-/-}$ outside dashed line ($n = 21$ for $Trpc1/4/5^{-/-}$, $n = 15$ for controls; $P < 0.0001$, two-way ANCOVA of type II).

D   Input–output curve of population spikes versus stimulation intensity ($n = 21$ for $Trpc1/4/5^{-/-}$, $n = 15$ for controls; $P = 0.0006$, two-way ANCOVA of type II). No significant differences between control and $Trpc1/4/5^{-/-}$ outside dashed line.

E   Baseline stimulation intensity used in LTP/depotentiation experiments in control and $Trpc1/4/5^{-/-}$ slices ($P = 0.0118$, t-test). Inset, baseline LFPs ($n = 21$ for $Trpc1/4/5^{-/-}$, $n = 15$ for controls; $P = 0.9906$, t-test).

F   "E-S curve" of LFP ("E") versus population spike ("S") of control slices at the first (black) and at the second (blue) pulse of a 50-ms paired pulse ($n = 13$ (9 mice); $P = 0.0011$, two-way ANCOVA of type II). No significant differences between first and second pulse outside dashed line.

G   "E-S curve" of $Trpc1/4/5^{-/-}$ at the first (red) and at the second (purple) pulse of a 50-ms paired pulse ($n = 18$ (10 mice); $P < 0.0001$, two-way ANCOVA of type II). No significant differences between first and second pulse outside dashed line. Of note, no difference in the first pulse between control (from F) and $Trpc1/4/5^{-/-}$ E-S curve ($P = 0.329$, two-way ANCOVA of type II).

H   LFP paired-pulse ratio (50-ms interstimulus interval) versus stimulation intensity ($n = 18$ (10 mice) for $Trpc1/4/5^{-/-}$, $n = 13$ (9 mice) for controls; $P = 0.0007$, two-way ANCOVA of type II) and versus the corresponding first pulse (inset, $P = 0.0724$, two-way ANCOVA of type II).

I   Baseline-normalized LFP versus time, before, and after 100-Hz stimulation (arrow 1) ($n = 21$ (10 mice) for $Trpc1/4/5^{-/-}$, $n = 15$ (10 mice) for controls). The first minute (**$P = 0.0066$, t-test on absolute LFPs) and the second minute (*$P = 0.0417$, t-test) after 100-Hz stimulation, control and $Trpc1/4/5^{-/-}$ are differently potentiated.

J   Baseline-normalized LFP versus time in one subset of (I), before and after 100-Hz stimulation (arrow 1). Both control ($P = 0.0136$, t-test on absolute LFPs) and $Trpc1/4/5^{-/-}$ ($P = 0.0033$, t-test on absolute LFPs) exhibit LTP ($n = 10$ (5 mice) for $Trpc1/4/5^{-/-}$, $n = 8$ (6 mice) for controls) with no difference in magnitude (relative LFP) between control and $Trpc1/4/5^{-/-}$ ($P = 0.1457$, Wilcoxon signed-rank test).

K   In the second subset of (I) baseline-normalized LFP versus time, at baseline, 5 min after 100-Hz stimulation (arrow 1), 15 min after 1-Hz paired-pulse (200 ms) stimulation (arrow 2; $P_{controls} = 0.0378$, $P_{TKO} = 0.0316$), and 20 min after 1-Hz paired-pulse (50-ms) stimulation (arrow 3; $P_{controls} = 0.2429$, $P_{TKO} = 0.2888$) ($n = 10$ (5 mice) for $Trpc1/4/5^{-/-}$, $n = 7$ (4 mice) for controls). CTR, control; TKO, $Trpc1/4/5^{-/-}$. Determination of the *P*-values is described in Materials and Methods.

Data information: Results are shown as mean ± SEM (shaded area or error bars).

position (Fig 8A). $Trpc1/4/5^{-/-}$ mice responded with a significant initial delay and an increased cumulative distance to the platform on the first training day, but learned on days 2 and 3 to find the hidden platform with similar efficiency as the controls. Strikingly, in the subsequent reversal part (tested on days 4 and 5), when the platform was moved to the opposite pool quadrant (Fig 8B and C), $Trpc1/4/5^{-/-}$ mice showed again significant deficits in platform localization, indicating impaired flexible spatial relearning of a new goal position.

To investigate whether the impaired performance of $Trpc1/4/5^{-/-}$ mice during relearning can be ascribed more tightly to hippocampus-dependent learning parameters, a qualitative analysis of defined search patterns was performed (Tsien *et al*, 1996b; Garthe *et al*, 2009). To unravel differences in navigational strategies between both genotypes, we defined categories of different swim patterns and applied a classification algorithm that allowed the automated classification in undirected search patterns including thigmotaxis, random search, scanning, and chaining on the one hand, and spatially more precise and thus hippocampus-dependent strategies on the other hand. Such directed, goal-oriented search strategies were categorized as "allocentric" search patterns and included directed search, focal search, and straight swimming, essentially as described (Garthe *et al*, 2009). To be able to apply such search strategies, mice have to form a coherent map of their environment, using the relations of the distant visual cues around the pool.

Allocentric strategies significantly increased as training progressed in controls already from days 1 to 2 and in $Trpc1/4/5^{-/-}$ from days 1 to 3. However, in contrast to the controls, $Trpc1/4/5^{-/-}$ mice did not show improvement in their allocentric performance from days 4 to 5 (Fig 9A and B). Furthermore, mutant mice

exhibited a substantially higher proportion of undirected, particularly thigmotactic, search behavior (dark green) throughout the entire test (Fig 9C). In addition, allocentric strategies (orange) were less frequently used by $Trpc1/4/5^{-/-}$ animals, suggesting that they navigate with lower spatial precision. These differences in search behavior became very prominent after relocating the platform during the reversal part of the test. Here, a random search pattern (blue) was used much more frequently by $Trpc1/4/5^{-/-}$ mice. The daily differences in delay to find the hidden platform were correlated with the deficits in the development of new efficient allocentric search strategies of TRPC1/4/5-deficient mice, indicating that $Trpc1/4/5^{-/-}$ animals stick to previously learned allocentric search strategies and are therefore impaired in relearning and behavioral flexibility (Fig 9D).

Discussion

In the present study, we demonstrate that TRPC1, TRPC4, and TRPC5 form heteromeric complexes in the brain and particularly in the hippocampus. Using $Trpc1/4/5^{-/-}$ as controls, we show the relevance of TRPC1/4/5 channels for synaptic transmission in cultured hippocampal neurons and hippocampal slices for working memory formation and in relearning tasks. Heteromultimer formation between TRPC1, TRPC4, and TRPC5 was established by co-immuno-precipitation of all three proteins with antibodies directed against each of them and the crucial isoform specificity of the employed antibodies confirmed by the use of the respective target-knockout controls. In previous heterologous co-expression experiments, TRPC1 proteins were shown to interact with all members of the TRPC subfamily, including TRPC3/6/7 subgroup (Storch *et al*,
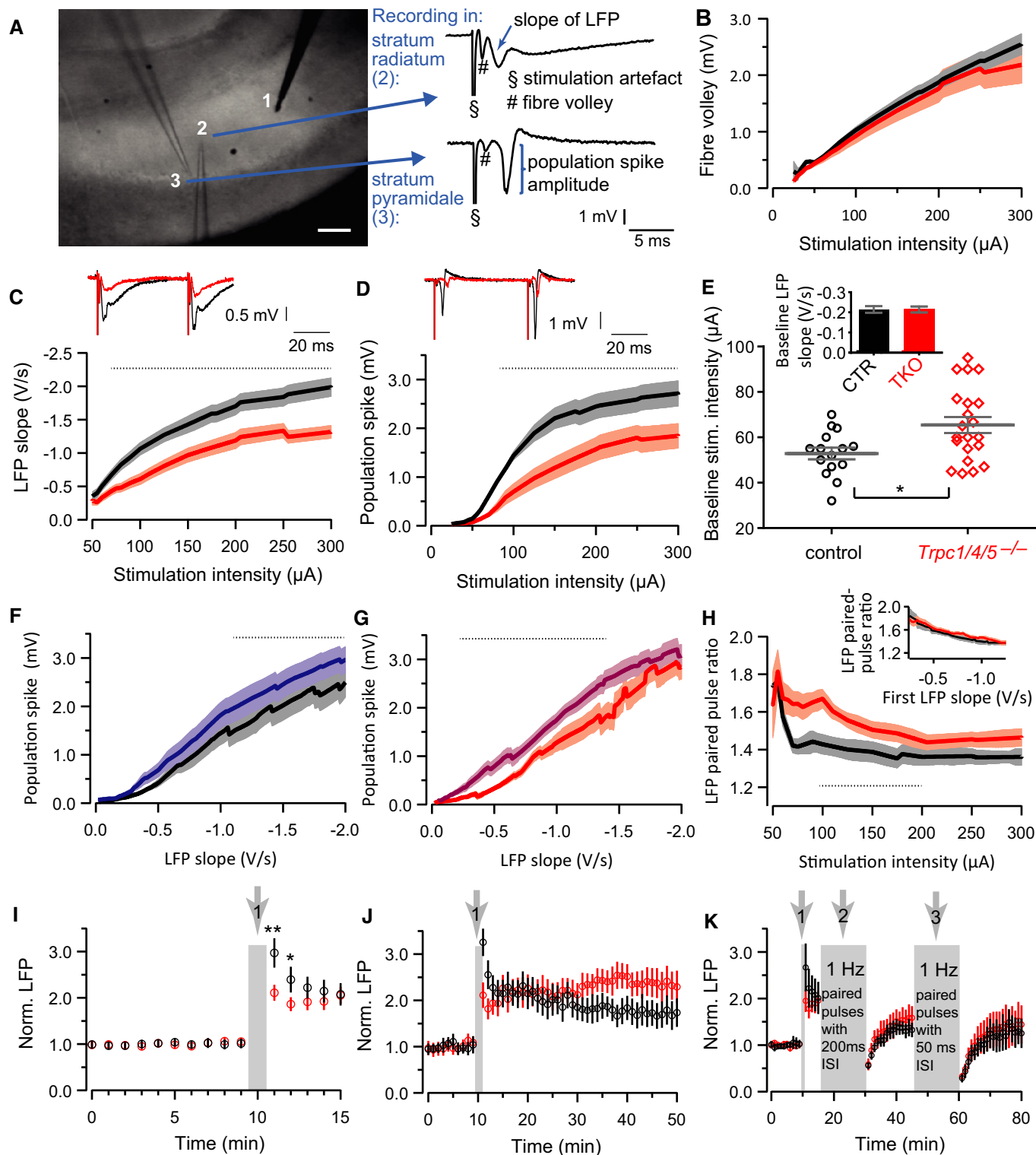
Figure 5.

2012) as well as with TRPV4 and TRPP2 (Ma *et al*, 2011; Du *et al*, 2014). In our experiments using MS-based protein detection, we neither found members of the TRPC3/6/7 subfamily, TRPV4 nor TRPP2 in affinity purifications of total brain or hippocampi with anti-TRPC1, anti-TRPC4, and anti-TRPC5 antibodies. Our results indicate the formation of heteromultimeric channels from TRPC1, TRPC4, and TRPC5 subunits, although the exact stoichiometry of such assemblies cannot be derived. Thus, TRPC1/4/5 channels may form ternary assemblies (TRPC1-C4-C5), as well as heteromers from two distinct subunits (TRPC1-TRPC4, TRPC1-TRPC5, TRPC4-TRPC5). The
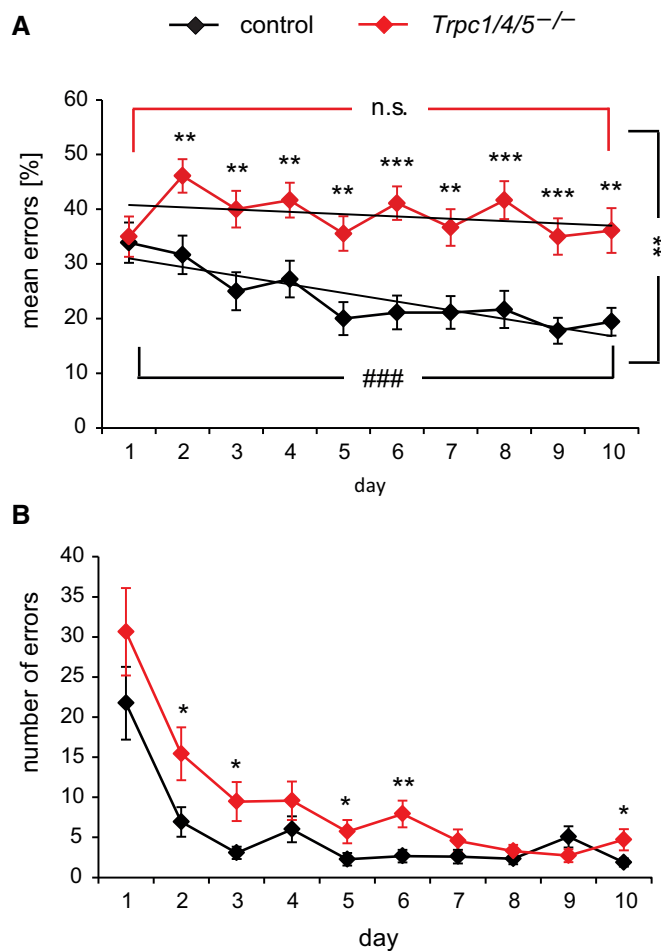
Figure 6. The deficiency of TRPC1, TRPC4, and TRPC5 impairs spatial working memory in the T-maze and radial maze tests.

A Number of errors per day in the delayed non-match-to-place T-maze task. $Trpc1/4/5^{-/-}$ mice (n = 30) perform consistently worse than the controls (n = 30; days 2–10 P < 0.0067, Mann–Whitney U-test). The maximum number of errors per day is 6. Analysis of the groups' individual performance curves confirms that the controls learn to alternate their choices of visited arms ($^{###}P$ < 0.001, Poisson regression with GEE) as the test progresses—unlike the $Trpc1/4/5^{-/-}$ animals. The learning curves of the two groups differ significantly ($^{**}P$ = 0.0015, Poisson regression with GEE).

B Number of errors per day in the radial maze test. During the early test phase, the animals lacking TRPC1, TRPC4, and TRPC5 exhibit a higher rate of mistakes (n = 15 for $Trpc1/4/5^{-/-}$, n = 14 for controls; days 2, 3, 5, 10 $^{*}P$ < 0.05, day 6 $^{**}P$ < 0.01).

Data information: Results are shown as mean ± SEM. $^{***}P$ < 0.001, $^{**}P$ < 0.01, $^{*}P$ < 0.05. The statistical tests are indicated for each comparison above., i.e. Mann–Whitney U-test or Poisson regression with GEE as indicated.

Figure 7. $Trpc1/4/5^{-/-}$ mice show a normal acquisition of spatial reference memory in the Morris water maze test.

A Schematic representation of the experimental procedure.

B, C The delay (B) and cumulative distance (C) to reach the platform during the acquisition phase are shown. The search performance of all animals is comparable (only day 2 $^{*}P$ < 0.02).

D Relative time spent in the four quadrants of the swimming pool without hidden platform during the probe trial. Mice of both genotypes spend significantly more time ($^{***}P$ < 0.001) in the training quadrant compared to the other three quadrants. SE quadrant: $^{*}P$ < 0.03.

Data information: Results are shown as mean ± SEM (n = 15 for $Trpc1/4/5^{-/-}$, n = 14 for controls). Statistical significance was determined using two-tailed unpaired Student's t-test.

formation of TRPC homomeric channels cannot be excluded by the results of the MS analysis either.

Functional analyses of synaptic transmission, using autaptic hippocampal neurons, revealed that the loss of TRPC1/4/5 channels significantly impaired action potential-evoked transmitter release. Furthermore, in neuronal mass cultures, the amplitude, charge, and kinetics of mEPSCs did not differ between $Trpc1/4/5^{-/-}$ neurons and controls, suggesting that TRPC1/4/5 channels are more supportive for action potential-dependent glutamate release.
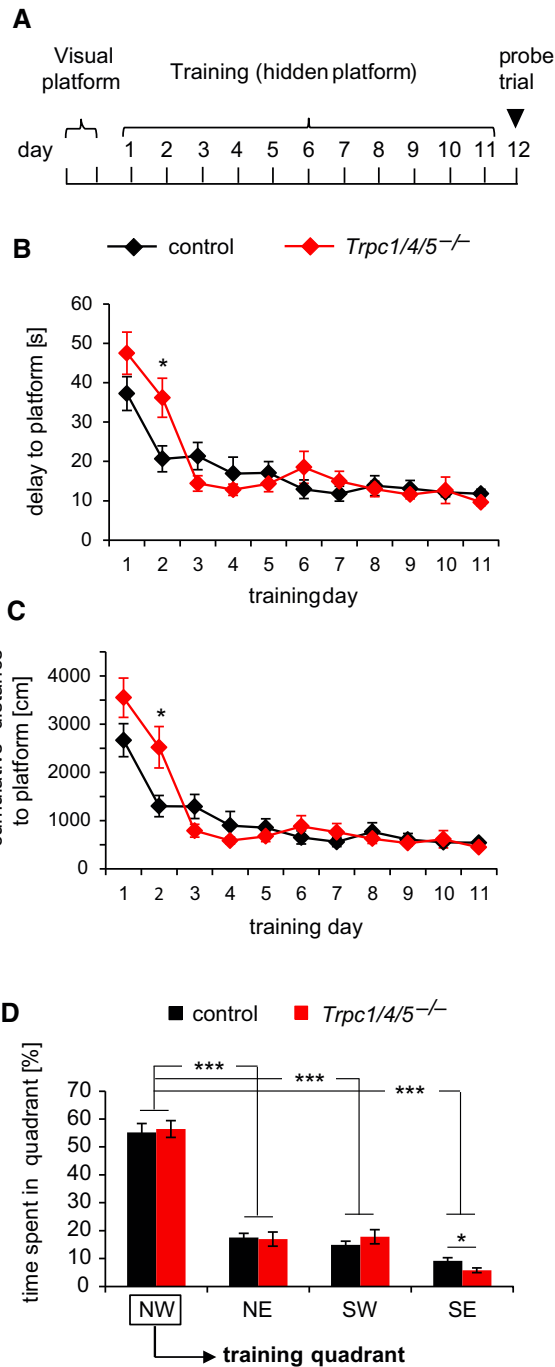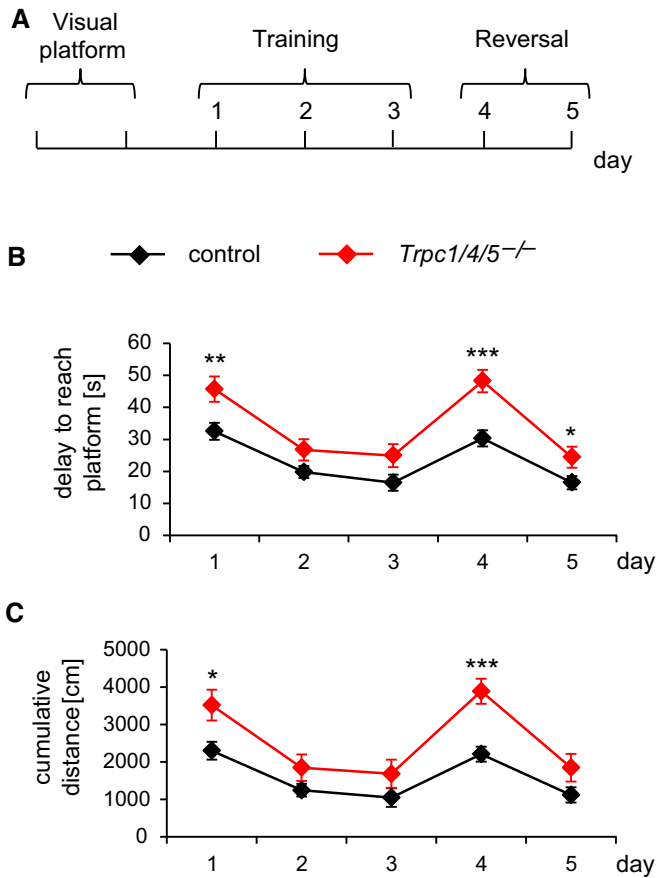
Figure 8. Impaired performance of *Trpc1/4/5*$^{-/-}$ mice in a modified Morris water maze test, assessing the competences of learning and relearning.

A   Schematic representation of the experimental procedure.

B, C   Mutant mice initially display increased delay (B) and cumulative distance (day 1 *P = 0.0129) (C) to the platform (day 1 **P = 0.0073), but comparable performances on the following two days show that both groups successfully learn to navigate to the hidden platform. TRPC1/4/5-deficient mice perform worse when they are challenged to relearn a new goal position in the reversal part (days 4, 5 $P < 0.05$) (n = 30 for *Trpc1/4/5*$^{-/-}$, n = 30 for controls). Results are shown as mean ± SEM. Statistical significance was determined using two-tailed unpaired Student's *t*-test; ***$P < 0.001$, **$P < 0.01$, *$P < 0.05$.

Moreover, synapse density was found to be unaltered in neuronal cultures of *Trpc1/4/5*$^{-/-}$. Overall, these results suggest that TRPC1/4/5 deficiency does not interfere with the postsynaptic glutamate response, but rather regulates excitability or Ca^{2+} homeostasis of presynaptic terminals.

Previous results have shown that TRPC 5 channels can be regulated/activated by intracellular Ca^{2+} elevations (Blair *et al*, 2009) at the millisecond time scale (Gross *et al*, 2009). Thus, an attractive scenario could be that synaptic Ca^{2+} influx via voltage-dependent Ca^{2+} channels is further enhanced by Ca^{2+}-dependent activation of synaptic TRPC channels, thereby leading to an overall increase in intracellular Ca^{2+}, which can powerfully regulate the pool size of release-ready vesicles (Stevens & Wesseling, 1998). Such a mechanism could also influence synaptic short-term plasticity (Dittman & Regehr, 1998; Wang & Kaczmarek, 1998; Lipstein *et al*, 2013).

In the same line, the results in acute hippocampal *Trpc1/4/5*$^{-/-}$ slices indicated impaired synaptic short-term plasticity (Fig 5H and I) that could contribute to the reduced efficacy of CA3-to-CA1 synapses. Both LFPs in the stratum radiatum and the postsynaptic firing of CA1 cells in the stratum pyramidale were reduced in *Trpc1/4/5*$^{-/-}$ preparations, compared to wild-type controls. These results point to an impaired postsynaptic firing of the CA1 neurons, due to decreased input by CA3 neurons. Yet, potential alterations, for example, in the number of active synapses cannot be rigorously excluded (Kerchner & Nicoll, 2008). Notably, the similar impact of TRPC1/4/5 deficiency on the evoked response in slice (Fig 5C) and culture experiments (Fig 2A and B) suggests that the deletion of *Trpc1*, *Trpc4*, and *Trpc5* affects glutamatergic transmission directly, rather than being mediated indirectly by altered GABAergic signaling in acute slices.

Similar findings on excitatory synaptic transmission were described in *Trpc5*$^{-/-}$ mice in neurons of the lateral amygdala of infantile (P13) mice, where EPSCs were reduced, the magnitude of paired-pulse facilitation was increased, and the amplitude of mEPSCs was unaltered (Riccio *et al*, 2009). However, synaptic strength analyzed from input–output curves for AMPA receptor-mediated EPSCs was unaltered at cortico-amygdala synapses and thalamo-amygdala synapses both in adolescent *Trpc5*$^{-/-}$ (Riccio *et al*, 2009) and in *Trpc4*$^{-/-}$ mice (Riccio *et al*, 2014). In contrast, cortico-amygdala and thalamo-amygdala EPSCs, mediated by group I mGluRs, were significantly diminished in slices from TRPC5 (Riccio *et al*, 2009) and in TRPC4-deficient animals (Riccio *et al*, 2014). As we show in this study, long-term potentiation (LTP) and subsequent depotentiation experiments in acute hippocampal slices did not show any significant differences in *Trpc1/4/5*$^{-/-}$ mice, supporting the regular postsynaptic function in the absence of TRPC1/4/5. In TRPC5-deficient mice, LTP was also not affected at cortico-amygdala synapses (Riccio *et al*, 2009), but was reduced at Schaffer collaterals, whereas *Trpc1*$^{-/-}$ and *Trpc1/Trpc4*$^{-/-}$ mice showed no significant impairments (Phelan *et al*, 2013). The reasons for these discrepant results remain unknown, but might be due to differences in *Trpc5* gene targeting strategies, genetic background of the mice, or experimental setups and design.

A major impairment of neuronal network activity in *Trpc1/4/5*$^{-/-}$ mice can be excluded by our study. The regular expression patterns of the AMPA receptor subunit GluA1 and the interneuronal key marker protein somatostatin suggest a normal neuronal connectivity in *Trpc1/4/5*$^{-/-}$ mice. Massive neuronal degradation can be ruled out by Nissl staining, as well as by NeuN and GFAP immunostaining. However, important structural changes might be discovered when stressing *Trpc1/4/5*$^{-/-}$ animals, subjecting them to disease models, or by more advanced morphologic analyses. For instance, impaired synaptic transmission might also be brought about by a reduction in morphological plasticity. The inactivation of TRPC4 was reported to result in an increase in neurite outgrowth and dendrite branching of hippocampal neurons (Jeon *et al*, 2013). Yet, similar results were obtained by the expression of a dominant-negative variant of TRPC5 (Greka *et al*, 2003), which renders the possibility of morphological alterations, underlying the observed changes in synaptic transmission unlikely, despite the fact that another study suggested that localized Ca^{2+} influx via TRPC5 channels promotes axon formation via activation of Ca^{2+}/calmodulin kinase kinase (CaMKK) and CaMKIγ (Davare *et al*, 2009). The integrity of neuronal
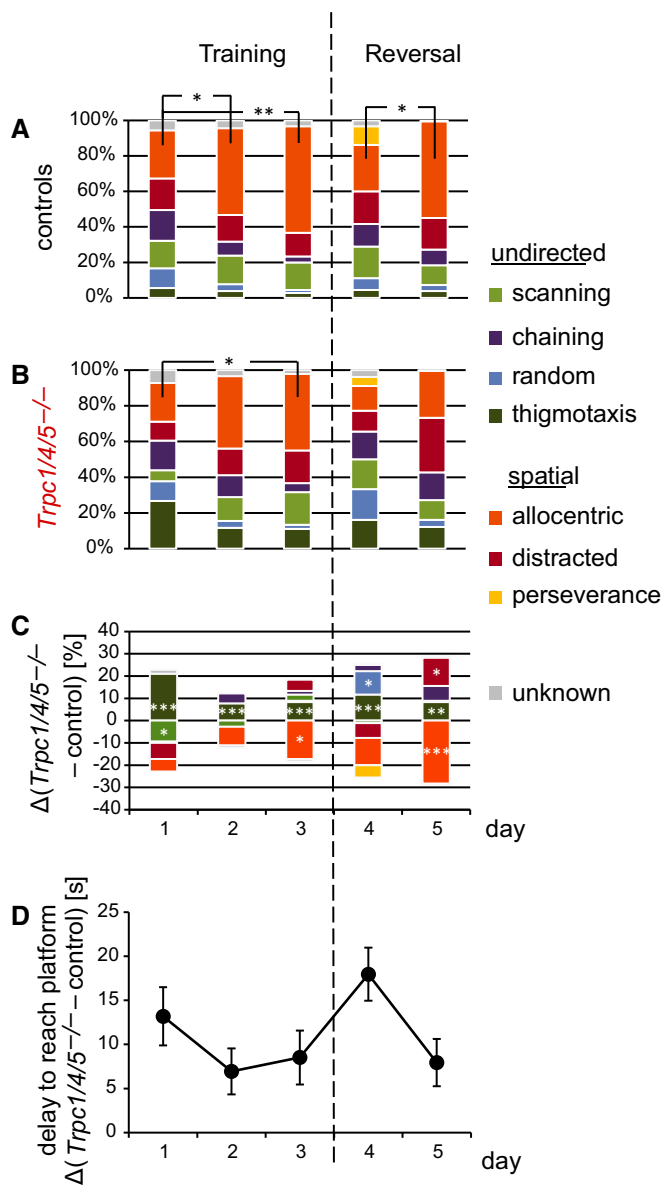
Figure 9. *Trpc1/4/5$^{-/-}$* mice exhibit less allocentric guided search strategies and more undirected search strategies in a modified Morris water maze test.

A, B   Qualitative analysis of search strategies used by controls and *Trpc1/4/5$^{-/-}$* mice. Mice of both genotypes show a progression in their search to allocentric (orange) strategies during the training phase (control: day 1 versus 2 *P = 0.02, day 1 versus 3 **P = 0.004; *Trpc1/4/5$^{-/-}$* *P = 0.01), but only the control animals change and improve their allocentric search behavior after relocation of the platform in the reversal part. *Trpc1/4/5$^{-/-}$* had difficulties to change and adapt new allocentric search behavior.

C   The proportion of individual search strategies of mutant mice was normalized to those of the controls. In *Trpc1/4/5$^{-/-}$* mice, the proportion of undirected swimming, especially thigmotaxis (dark green), is increased (days 1–5 ***P < 0.001), and allocentric strategies (orange) are less frequently used (day 3 *P = 0.03, day 5 ***P < 0.001). Notably, they also exhibit more often a random swim pattern (blue) during the reversal phase of the test (*P = 0.04).

D   Mean difference between the groups in delay to the hidden platform correlates with deficits in efficient search modes (n = 30 for *Trpc1/4/5$^{-/-}$*, n = 30 for controls). Results are shown as mean ± SEM.

Data information: Statistical significance was determined using two-tailed unpaired Student's *t*-test; ***P < 0.001, **P < 0.01, *P < 0.05.

network function in TRPC1/4/5-deficient mice finds further support in unchanged basal parameters of typical network patterns as concluded from unaltered theta and gamma oscillations. However, cross-frequency phase–amplitude coupling (CFC) was impaired in *Trpc1/4/5$^{-/-}$* animals. Coordination between slow and fast network oscillations has been suggested to underlie complex mnemonic processes, including working memory tasks (Wulff *et al*, 2009; Korotkova *et al*, 2010). The observed impairment of CFC in *Trpc1/4/5$^{-/-}$* mice might therefore causally contribute to the mnemonic deficits discussed below.

TRPC1/4/5-deficient animals are housed as an inbred mouse line. They breed and the number of offspring is normal, without showing any signs of early death. Additionally, the behavioral SHIRPA analysis of *Trpc1/4/5$^{-/-}$* mice did not reveal any impairment in spontaneous activity, body position, and tremor, vision, and hearing. The rotarod test showed that the genetic deletion of *Trpc1*, *Trpc4*, and *Trpc5* did not result in impaired walking behavior, as it has been described for *Trpc3$^{-/-}$* mice (Hartmann *et al*, 2008). Moreover, intact spatial reference learning and memory in two different versions of the Morris water maze show that the ubiquitous and constitutive genetic inactivation of *Trpc1*, *Trpc4*, and *Trpc5* does not impair spatial reference learning as described for hippocampal lesions (Morris *et al*, 1982, 1990; Aggleton *et al*, 1986; Logue *et al*, 1997; Arns *et al*, 1999; Deacon *et al*, 2002; Broadbent *et al*, 2004).

In contrast to our results, Xing *et al* have suggested impairments in spatial memory, due to the genetic ablation of *Trpc1* (Xing *et al*, 2016). However, the unconventional Y-maze protocol applied in the study of Xing *et al* does neither specifically assess spontaneous alternation, spatial working, nor reference memory, as it has been reliably shown by other groups (Hughes, 2004; Fuchs *et al*, 2007). Also, the fear conditioning results of Xing *et al* cannot be related to any (spatial) memory deficits, since *Trpc1$^{-/-}$* mice already showed markedly less freezing during the acquisition phase. Moreover, the deficits of *Trpc1$^{-/-}$* mice in the step-down inhibitory avoidance task are rather ambiguous, because the test does not only assess hippocampus-related long-term memory formation, but has also been associated with amygdala-dependent anxiety-like behavior (Izquierdo & Medina, 1997; Collins *et al*, 2012).

The performance of *Trpc1/4/5$^{-/-}$* mice in the T-maze and radial maze uncovered distinct SWM deficits in TRPC1/4/5-deficient animals. *Trpc1/4/5$^{-/-}$* mice also differed from controls in their competence to use precise and allocentric search strategies during the acquisition in the reversal learning version of the Morris water maze. *Trpc1/4/5$^{-/-}$* animals exhibited a substantially higher proportion of undirected search patterns during the daily trials, demonstrating that *Trpc1/4/5$^{-/-}$* mice are impaired in recalling efficiently successful search strategies from previous trials on that day. Nevertheless, *Trpc1/4/5$^{-/-}$* mice learned the position of the submerged platform in the Morris water maze, indicating that SRM is operative in the absence of TRPC1/4/5.

Interestingly, Pereira and Wang (2015) demonstrated that the accuracy and robustness of intact working memory is enhanced by the activation of calcium-dependent nonspecific cationic currents (I$_{CAN}$), which are reminiscent of TRPC-mediated currents. These observations are in line with the deficiencies we delineated in synaptic plasticity in acute hippocampal slices of *Trpc1/4/5$^{-/-}$* mice and mnemonic behavior.

Mice lacking TRPC1/4/5 also exhibited significant deficiencies to adapt to new challenges in the relearning paradigm of the Morris water maze. Thus, the memory for the submerged platform in the Morris water maze seems to be more stable in $Trpc1/4/5^{-/-}$ mice. A more stable SRM, in the absence of SWM, was also noticed in a classical mouse model with strong impairment in SWM, the GluA1-knockout mice ($Gria1^{-/-}$) (Zamanillo *et al*, 1999). In $Gria1^{-/-}$ mice, the SWM was impaired in the T-maze, whereas the acquisition of SRM in the Morris water maze and radial maze was still intact (Zamanillo *et al*, 1999; Reisel *et al*, 2002). Moreover, GluA1-deficient mice show more stable SRM for previously visited locations (Sanderson *et al*, 2009). Thus, the delay in SRM relearning in $Trpc1/4/5^{-/-}$ mice can be taken as an additional indicator that TRPC1/4/5-deficient animals suffer from short-term spatial memory deficiencies. A very similar learning impairment was described for mice lacking the receptor subunit GluN2A ($Grin2a^{-/-}$) of hippocampal NMDA receptors ($Grin1^{\Delta DGCA}$) (Bannerman *et al*, 2008, 2012). In contrast to previous findings that $Grin2a^{-/-}$ mice suffer from SRM deficits, a subsequent detailed analysis of $Grin2a^{-/-}$ concluded that the NMDA receptor GluN2A is required for rapidly acquired SWM, but not incremental SRM (Bannerman *et al*, 2008), reminiscent to the learning phenotype of $Trpc1/4/5^{-/-}$ mice. Likewise, $Grin1^{\Delta DGCA1}$ mice that lack NMDA receptors in hippocampal pyramidal CA1 neurons and DG granule cells exhibited no deficit in the acquisition of SRM when analyzed in the classical Morris water maze or the beacon water maze (Bannerman *et al*, 2012). In these $Grin1^{\Delta DGCA1}$ mice, the relearning of a novel platform position in the Morris water maze was impaired, which was interpreted as a lack of behavioral flexibility (Bannerman *et al*, 2012; Bannerman *et al*, 2014). Despite the very similar spatial learning impairments of $Trpc1/4/5^{-/-}$, $Gria1^{-/-}$, $Grin2a^{-/-}$, and $Grin1^{\Delta DGCA1}$ mice, only the $Gria1^{-/-}$, $Grin2a^{-/-}$, and $Grin1^{\Delta DGCA1}$ show strong impairments in LTP at hippocampal synapses (Zamanillo *et al*, 1999; Steigerwald *et al*, 2000; Kohr *et al*, 2003; Bannerman *et al*, 2012). In $Tpc1/4/5^{-/-}$ mice, the hippocampal synaptic plasticity appears to be normal in LTP and in corresponding depotentiation measurements, supporting the view that the LTP analysis in acute hippocampal slices might not represent an *ex vivo* evaluator for hippocampal function *in vivo* (Neves *et al*, 2008).

Our findings render the interaction between TRPC1/4/5 and these ionotropic NMDA or AMPA glutamate receptors to be unlikely, although TRPC1 and TRPC4 are apparently activated downstream of NMDA receptor activation in granule cells of the mouse olfactory bulb (Stroh *et al*, 2012). Alternatively, it has been proposed that TRPC channels might underlie group I metabotropic glutamate receptor (mGluR)-dependent conductance in CA3 pyramidal neurons (Kim *et al*, 2003; Hartmann *et al*, 2008; Wu *et al*, 2010). This idea is supported by the observations that the lack of TRPC1 and TRPC4, but not of TRPC5 proteins, abolished the burst firing induced by mGluR activity in lateral septum neurons (Phelan *et al*, 2012, 2013). Previous studies using group I mGluR agonists, antagonists, or toxins that reduce mGluR expression have assigned a critical role for spatial learning and memory formation to mGluR (Riedel & Reymann, 1996; Balschun *et al*, 1999; Ayala *et al*, 2009; Jiang *et al*, 2014). But a conclusive mechanistic link between the involvement of TRPC proteins in mGluR-mediated synaptic transmission and their function in hippocampus-dependent behavior will require further in-depth studies.

In summary, our data provide novel evidences that TRPC1, TRPC4, and TRPC5 interact in the brain and hippocampus. Based on electrophysiological recordings at hippocampal synapses, these TRPC subunits are crucially involved, likely presynaptically, in the efficiency of synaptic plasticity and neuronal network communication, and might, thereby, participate in spatial working memory and flexible spatial relearning.

Materials and Methods

Ethics statement

All experimental procedures were approved and performed in accordance with the ethic regulations and the animal welfare committees of the Universities of Saarland and Heidelberg. All efforts were made to minimize animal suffering and to reduce the number of animals used.

Animals

A triple-knockout mouse line $Trpc1/4/5^{-/-}$ was generated by intercrossing mice of the three mouse lines—$Trpc1^{-/-}$ (Dietrich *et al*, 2007), $Trpc4^{-/-}$ (Freichel *et al*, 2001), and $Trpc5^{-/-}$ (Xue *et al*, 2011). Each had been backcrossed to the C57Bl6/N strain (Charles River) for at least seven generations before they were used to generate the $Trpc1/4/5^{-/-}$ line. C57BL6/N control mice were obtained from Charles River and housed in the same animal facility as the $Trpc1/4/5^{-/-}$ mice.

Biochemistry/proteomic analysis

Affinity purification

Membrane fractions from hippocampi and whole brains of adult wild-type controls, and membrane fractions from whole brains of adult $Trpc1^{-/-}$, $Trpc4^{-/-}$, $Trpc5^{-/-}$-single-knockout, or $Trpc1/4/5^{-/-}$-triple-knockout mice were prepared as previously described (Sailer *et al*, 2002) and solubilized with ComplexioLyte 47 (CL-47, Logopharm GmbH) for 30 mins on ice (at a concentration of 1.25 mg/ml). After clearing by ultracentrifugation (10 mins, $125,000 \times g$, 4°C), the solubilized protein was incubated for 2 h on ice with anti-TRPC1 (ab4921), anti-TRPC4 (ab1377), or anti-TRPC5 (ab777 EB) antibodies, generated in-house, and cross-linked to Protein A Dynabeads (LifeTechnologies). Beads were washed twice with CL-47 dilution buffer (Logopharm GmbH), and bound protein was eluted with non-reducing Laemmli buffer at 37°C.

Data analysis

MS/MS analysis was done as detailed in Schwenk *et al* (2014). Briefly, eluted proteins were subjected to an in-gel tryptic digest. Nano-LC-MS/MS analyses were performed using an UltiMate 3000 HPLC and a LTQ Orbitrap XL mass spectrometer (both Thermo Scientific). Peak lists were extracted with "msconvert.exe" (part of ProteoWizard; http://proteowizard.sourceforge.net/; version 3.0.6906; default Mascot Daemon filter options) and—after pre-search and linear shift mass recalibration—finally searched against all mouse, rat, and human entries (including P00761|TRYP_PIG, P00766|CTRA_BOVIN, and P02769|ALBU_BOVIN) of UniProtKB/Swiss-Prot (release 2016_08)

with Mascot 2.5.1 (Matrix Science; search parameters as described in Schwenk *et al* (2014).

Protein abundance ratios in anti-TRPC affinity purifications (versus IgG controls) were calculated as described in Schwenk *et al* (2016). Peak volumes (PV) of individual peptides were determined by in-house written software and are provided in Dataset EV1. Relative protein abundance ratios were calculated by the TopCorr method (Bildl *et al*, 2012), computing the median of PV ratios for the two to six best correlating protein-specific peptides.

Electrophysiological recordings in autaptic neurons

Autaptic cultures of hippocampal neurons were prepared at P1-2 from *Trpc1/4/5$^{-/-}$* mice, as described (Bekkers & Stevens, 1991; Schoch *et al*, 2001; Guzman *et al*, 2010). Hippocampi were dissected from brain and digested for 20 mins at 37°C with 10 units of papain (Worthington, USA), followed by gentle mechanical trituration. Neurons (density 1,000 cells/ml) were seeded onto a layer of glial microislands, resulting in a co-culture of glia and nerve cells. Only islands containing single neurons were used for electrophysiology. For mass cultures, neuronal cell suspensions were plated at low density (300 cells/mm^2) on 25-mm cover slips coated with 0.5 mg/ml of poly-D-lysine (Sigma). Cultures were maintained at 37°C in an incubator, humidified with 95% air and 5% CO_2 in NBA (Invitrogen), supplemented with 2% B-27 (Sigma), 1% Glutamax (Invitrogen), and 2% penicillin/streptomycin (Invitrogen). Recordings were performed at room temperature on days 14–17 of culturing.

Whole-cell voltage-clamp recordings of synaptic currents were obtained from isolated autaptic neurons. All experiments include measurements from more than three different culture preparations and were performed in parallel with age-matched neurons derived from C57Bl6/N wild-type mice. Patch pipettes (4–5 MΩ) were filled with intracellular solution containing (in mM): 137.5 K-gluconate, 11 NaCl, 2 MgATP, 0.2 Na$_2$GTP, 1.1 EGTA, 11 HEPES, 11 D-glucose, pH 7.3. The standard extracellular solution consisted of (in mM) 130 NaCl, 10 NaHCO$_3$, 2.4 KCl, 4 Ca^{2+}, 4 MgCl$_2$, 10 HEPES, 10 D-glucose, pH 7.3 with NaOH, osmolarity 300 mOsm. Neurons were voltage-clamped at −70 mV with an EPC10 amplifier (HEKA Electronik) under the control of the Pulse 8.5 program (HEKA Electronik) and stimulated by membrane depolarizations to +10 mV for 0.7 ms every 5 s (0.2 Hz). Current signals were low-pass-filtered at 2.9 kHz. For recording spontaneous miniature EPSCs (mEPSCs), mass cultures of hippocampal neurons were bathed in Ringer's solution, containing 1 μM tetrodotoxin (TTX). To minimize the clamp error, cells with access resistances of < 10 MΩ and with 80–85% resistance compensation were analyzed. To determine the mEPSC properties with reasonable fidelity, spontaneous events with a peak amplitude > 15 pA (~5 times the SD of the background noise and a charge criterion > 25 fC) were analyzed using a commercial software (Mini analysis, Synaptosoft, version 6.0.3).

Electrophysiological recordings in brain slices

Adult mice (14–22 weeks) were anesthetized and transcardially perfused with sucrose saline. Acute transverse slices (280 μm) from the middle hippocampus were cut and stored in a submerged chamber with sucrose saline (in mM: 87 NaCl, 25 NaHCO$_3$, 2.5 KCl, 1.25

NaH$_2$PO$_4$, 7 MgSO$_4$, 0.5 CaCl$_2$, 10 glucose, 65 sucrose, 0.01 sodium pyruvate bubbled with 95% O$_2$/5% CO$_2$, ~300 mOsm). Schaffer collaterals (CA3 axons) were stimulated every 20 s with a 1-μm-tip monopolar tungsten electrode (WPI) by biphasic electrical stimulation in stratum radiatum (~300 μm shifted toward CA3). With two glass pipettes filled with 1 M NaCl, local field potentials (LFPs) were recorded in stratum radiatum and the corresponding population spikes were recorded in stratum pyramidale in current clamp (EPC10, HEKA Elektronik, Patchmaster software), as shown in Fig 5A. Acute slices were perfused at 33°C in a submerged recording chamber with saline (in mM: 125 NaCl, 25 NaHCO$_3$, 2.5 KCl, 1.25 NaH$_2$PO$_4$, 1 MgCl$_2$, 2 CaCl$_2$, 13 glucose, bubbled with 95% O$_2$/5% CO$_2$, ~300 mOsm). Slopes of LFPs were determined by the slope of a 30–70% linear fit; amplitudes of population spikes (negative deflection) were determined relative to baseline. Paired-pulse LFPs were evoked during input–output curves with an interstimulus interval of 50 ms, but not during plasticity experiments.

Data analysis
Data were analyzed in Igor Pro 6.37 (Wavemetrics). Results are shown as mean ± SEM. Statistical significances were assessed in GraphPadPrism 5.02 or in R 3.3.2 (package "car", version 2.1-3). In plasticity experiments (Fig 5I–K), the absolute LFP slopes of the respective experiments were compared between 10-min baseline average and the average of the last 5 mins after the respective plasticity induction by a paired *t*-test. Statistical differences in the categorical independent factor "genotype" (Fig 5C, D and H) or "first" versus "second paired pulse" (Fig 5F and G) were tested with two-way ANCOVA of type II, implemented in R. The respective continuous dependent response (from the *y*-axis) and the second independent (continuous) factor (from the *x*-axis) were taken into account for this analysis.

Electrophysiological recordings *in vivo*

Animal care and housing conditions
Animals were housed in groups of up to four, inside a ventilated Scantainer (Scanbur BK) on an inverted 12-h light/dark cycle (light on at 8:00 P.M.). All animals had free access to food and water. After chronic electrode implantation, animals were housed individually throughout the experiment. After behavioral experiments, animals were killed with an overdose of isoflurane.

Surgery procedure
A total of 10 male animals, aged between 10 and 14 weeks, weighing ~20–24 g were anesthetized with isoflurane and medical oxygen (4% isoflurane for induction, 1.0–2.0% for maintenance, flow rate: 1 l/min). For analgesia, 0.1 mg/kg of buprenorphine hydrochloride was subcutaneously injected prior and 8 h after surgery. Anesthetized animals were head-fixed on a stereotaxic apparatus (David Kopf Instruments) with a custom-made inhalation tube. Body temperature was kept stable at 37–38°C with a heating pad underneath the animal's body (ATC-2000, World Precision Instruments). After exposure of the skull, holes of a diameter of 0.6 mm were drilled according to stereotaxic coordinates (Paxinos & Franklin, 2001). Two octrodes (eight twisted wires) were implanted into the right and left dorsal CA1 region (AP +/− 1.94 mm, ML +/− 1.25 mm, DV −1.1 mm), and two brass watch stainless steel screws

(M1x3) were implanted into the cerebellum to serve as reference and ground electrode, respectively. After surgery, animals were allowed to recover for 7 days.

Electrophysiology

We recorded LFPs from the dorsal hippocampal CA1 region of freely moving mice. In addition to electrophysiological recordings, three accelerometers registered translational movements in x, y, and z directions. One week after surgery, recordings were performed for 5 h in the animal's home cage (see Fig 4A). Extracellular signals were filtered (1–500 Hz), amplified (RHA2116, Intan Technologies), digitized (2.5 kHz), and stored for offline analyses with custom-written MATLAB routines (The MathWorks).

Behavioral staging

We restricted our analyses to selected rapid eye movement sleep phases (REM), where both characteristic and robust theta-nested gamma oscillations (4–12 Hz and 30–140 Hz) occur. REM sleep was identified by the absence of movement on all accelerometers accompanied by prominent regular theta oscillations.

Spectral analysis

Power spectral density analysis was calculated by means of the Welch periodogram method using the pwelch.m function from the Signal Processing Toolbox of Matlab (50% overlapping, 4-s Hamming windows).

Cross-frequency coupling analysis

To measure the intensity of coupling between the phase of a slow oscillation and the amplitude of a fast oscillation, we computed the modulation index (MI, for details see Tort *et al* (2008)). In brief, the MI is a measure to evaluate the divergence of phase–amplitude coupling from a uniform distribution, normalized such that values range between 0 (no coupling) and 1 (maximal coupling). We next selected the MI peaks to evaluate the maximum MI values of low gamma and high gamma to theta coupling, respectively, for further statistical analyses.

Immunostaining in hippocampal neurons

Mass neuronal cultures were fixed for 30 mins at room temperature in PBS containing 4% paraformaldehyde and 4% sucrose. Cultures were quenched for 10 mins with 50 mM NH_4Cl in PBS, blocked for 1 h in PBS containing 3% BSA, and 0.1% Triton X-100. Primary and secondary antibodies were diluted in 3% BSA, 0.1% Triton X-100 in PBS. Cells were incubated with primary antibodies anti-synaptophysin (mouse monoclonal, Synaptic Systems, Germany) overnight. After rinsing, they were incubated once with PBS containing 4 M NaCl, then washed briefly in PBS. Alexa-Fluor 543 (Invitrogen) was applied for 2 h. After washing in PBS, cells were imaged immediately or mounted on 2 μl glycerol. Epifluorescence pictures were digitized with an AxioCam MRm-CCD camera (Zeiss) at the focal plane of the axonal network with a 25× and 100× objective (Zeiss). Images were acquired with the software Axiovision 4.5 (Zeiss) and analyzed with Metamorph software (Universal Imaging Inc.). Immunopositive spots were determined using a threshold-based detection routine, with the threshold adjusted to the background signal of the dendrite. Immunosignals were quantified as mean

fluorescent intensity. For the analysis of synaptic density, synapto-physin-positive puncta were counted along 50 μm dendrite length (Guzman *et al*, 2010).

Histochemistry and immunostainings in brain slices

Experimentally naive 14-week-old mice were anesthetized with isoflurane and transcardially perfused with PBS as well as 4% paraformaldehyde (PFA; Roti®-Histofix 4%, Roth). Prior to and after the postfixation with PFA in PBS (4°C) for 1.5 h, brains were washed in PBS and then embedded in 2% agarose (in PBS). Coronal sections (100 μm) were cut on a vibratome (Leica VT1000S) and kept in PBS. For the immunostaining, they were first pretreated with 0.5% H_2O_2 (Fluka Analytical) in PBS for 15 mins to quench endogenous peroxidase activity, followed by Solution D1 (1% albumin from bovine serum (BSA; Sigma), 0.3% Triton X-100 (Sigma) in PBS) supplemented with 2% normal goat serum (NGS; Invitrogen) to block unspecific protein binding sites. Several washing steps with PBS were performed in between. After 1 h, brain slices were incubated with primary antibodies overnight. The dilutions were prepared in D1 and consisted of rabbit antibody targeting either GluA1 (1:1,000; abcam®), glial fibrillary acidic protein (GFAP; 1:500; DakoCytomation), or somatostatin (1:400; abcam®) or mouse antibody targeting NeuN (1:1,000; Millipore®). On the next day, after rinsing with D2 (0.33% BSA (Sigma), 0.1% Triton X-100 (Sigma) in PBS), the sections were incubated for 1 h with peroxidase-labeled anti-rabbit IgG secondary antibody (Vector), diluted 1:600 in D2, followed by washing steps. Slices were then stained with diaminobenzidine solution (0.4 mg/ml DAB in 20 mM Tris (pH 7.6) and 30% H_2O_2). The reaction was stopped with PBS. Stained sections were mounted onto glass slides using 10 mM Tris (pH 7.6). After drying, slices were embedded in xylene (Merck) with Eukitt® quick-hardening mounting medium (Fluka Analytical). All staining processes were performed at room temperature. For Nissl staining, brains were taken from experimentally naive 14-week-old mice, immediately frozen on dry ice, and stored at −80°C. Transverse sections (12 μm) were cut at −20°C on a cryostat (Leica CM3050 S) and mounted onto microscope slides, previously coated with poly-L-lysine. Slides were kept at −20°C. Brain sections were dried at room temperature for 2–3 h before they were incubated for 140 s in thionine solution (0.1% thionine in 0.1 M acetic acid and 0.1 M Na-acetate, filtered) and rinsed with distilled water. After drying, slices were embedded in xylene with Eukitt®. Bright field images of DAB- and Nissl-stained slices were taken with the Axio Imager M1 (10× magnifying objective, Zeiss) using the Zeiss Axiovision software.

Behavioral assays

Animals were housed in an animal facility with a regular 12-h light/dark cycle (light on at 7:00 A.M.). Food and water was supplied *ad libitum*, unless the mice were kept on a food-restricted diet during an appetite-motivated learning task (T-maze, radial maze tests). All behavioral tests were conducted with counterbalanced, gender-, and age-matched groups (two- to 4-month-old male and female adults). We compared C57Bl6/N wild-type and *Trpc1/4/5*$^{-/-}$ mice. Different tests were performed on different days.

SHIRPA (SmithKline Beecham, Harwell, Imperial College, Royal London Hospital, phenotype assessment)

Mice were placed in a corner of a clear Plexiglas box and allowed to explore for 30 s. For the evaluation of spontaneous behavior, the body position (lying, sitting, rearing), activity (from immobile to extreme movement), body tremor, twitches, number of urine puddles, and fecal boli were taken into consideration. Vision was tested by lowering the mouse onto a wire grid by the suspension of its tail. The relative distance to the grid at which the animal started to extend its forelimbs was used as a criterion for visual placing responses. Hearing skills were assessed by exposing the mouse directly to a loud sound made by a rubber glove. Sudden twitches were counted as a positive reaction. Tested reflexes included corneal, pinna, or toe pinch reflex. Eye blinking, and active retraction of the ear or the withdrawal of the hindlimbs, respectively, was expected.

Rotarod

In the rotarod experiment, a rod rotated at a gradually increasing speed. It initially turned at 4 rpm, going up to 40 rpm over a period of 8 mins. The time the animal was able to maintain itself on the rotating rod was measured to judge motor coordination. Mice were subjected to three runs per day (intertrial interval: 15 mins) on 2 days with a 1-day break in between.

Delayed non-match-to-place T-maze

The apparatus was an enclosed T-shaped maze constructed of gray Plexiglas. Every arm was $7 \times 10 \times 28$ cm. Throughout the entire test period, animals were kept on a food-restricted diet to motivate them for the food-rewarded task. Providing ~2 g of pellets per mouse every day, 85–90% of the initial body weight was maintained. At all times, access to water was unlimited.

Over 4 days, the animals were habituated to the maze in four runs per day. In each run, they were allowed to explore one given goal arm. At its end, they were rewarded with a 2-mg pellet of food, composed of 61.5% carbohydrate, 18.5% protein, 4.9% fat, 4.5% fiber (caloric value: 3.62 cal/mg). The opposing goal arm was closed by inserting a gray Plexiglas divider. During the four runs, the accessible goal arms were randomly alternated. If the mouse had not found the pellet within 120 s, the animal was put back to its home cage. The intertrial interval for each habituation run was ~10 mins. Over the following 10 days, mice performed six trials per day, with a 20-min intertrial interval. Each trial was composed of two runs in the T-maze. During the first run (test run), the unrewarded arm was blocked and the animal could only enter the food-rewarded goal arm. After 10 s, the mouse was placed back to the start arm for the second (free choice) run. In the free choice run, both goal arms of the T-maze were accessible, but only the previously blocked (alternative) arm contained a food pellet. It was considered an error, when the mouse entered the same arm in the test and free choice run of one trial. The trial was valued as successful if the pellets in both arms were taken. Entering an arm with all four paws was counted as choice. The cutoff time per run was again 2 mins.

Radial maze

The apparatus consisted of eight equally sized enclosed arms ($5.5 \times 6 \times 27.5$ cm) made of gray Plexiglas with transparent lids and walls. These arms were assembled in a radial manner around a circular starting platform. The animals were kept on a food-restricted diet with unlimited access to water, maintaining 85–90% of their pre-test body weight. Habituation: On two successive days, all eight arms were open and baited with a couple of oat flakes. Each mouse was given 10 mins to familiarize itself with the environment. Then, the animals were tested on 10 consecutive days with one trial per day with all eight maze arms being open. For each mouse, a specific set of four arms was baited with an oat flake; the other four arms were always unbaited. For every animal, always the same four arms were baited throughout the test. In contrast to the habituation, now only one oat flake was placed behind a low barrier to prevent the mice from seeing whether or not a certain arm was still baited before entering it completely. Some flakes were deposited behind a perforated wall at the very end of each arm. This way, the animals could not distinguish between the presence and absence of the food reward by smelling. Several extra-maze cues, whose position remained constant throughout the experiment, were provided close to the arms. The maze arms were exchanged after every trial to avoid the use of aromatic cues for orientation. The trial was stopped after all four food rewards were eaten or after 10 mins. Every repeated entry into a previously visited arm was counted as a working memory error.

Morris water maze experiment and pattern analysis

The apparatus was a circular gray metal pool (diameter: 180 cm; AnyMaze 60235, USA) filled with water ($22 \pm 1°C$) that was made opaque by adding TiO_2 and frequent stirring between trials. The circular white escape platform (diameter: 10 cm) was submerged 1 cm below the water surface in the middle of the goal quadrant. Extra-maze cues were positioned around the pool. Sygnis Tracker software was used to measure swim path length, latency to reach the platform, time spent in each quadrant, and cumulative distance to the platform. If a mouse failed to reach the goal within 90 s, it was guided there manually. After mounting the platform, the animal remained there for 10 s.

For 2 days, the animals were subjected to a visual platform task. Here, a protruding colorful grid made the platform visible. The maze was covered with black curtains to hide the room cues. In each of the four runs per day (intertrial interval: 30 mins), the platform was placed in a different quadrant, while the swimming start position was always diagonal to the platform location.

Spatial reference memory version (Malleret *et al*, 1999) On 11 days following the visual platform task, mice were trained to find the hidden platform by using the visual cues surrounding the pool; that is, the colorful grid and the black curtains were removed. Throughout the entire training, the platform remained in the same position (upper left quadrant). The animals performed four runs per day, each starting from a different position along the pool wall (E, SE, S, and SW). The order of the starting positions was chosen randomly but remained the same for all mice throughout a training day. The subsequent probe trial on day 12 consisted of one 120-s trial in opaque water without any platform. The starting direction was farthest away from the "platform" quadrant (SE).

Reversal learning version (Garthe *et al*, 2009) Two days of habituation (visual platform task, see above) were directly followed by

3 days of training and 2 days of reversal learning. Each mouse was given six trials per day. Throughout 1 day, the starting position remained the same, but it was changed every day. During the reversal part, the platform was moved from the upper left (training) to the lower right quadrant.

The analysis of the search strategies allowed a qualitative estimation of the learning process during the Morris water maze task (Garthe *et al*, 2009). The following categories were defined according to specific criteria, such as time spent or distance traveled in a specific pool region: "Thigmotaxis" describes slow swimming close to the pool wall. The swim path of a "random search" pattern covers a large portion of the pool. During "scanning", the animal swims mainly in the central area, where it can see the distant visual cues best and where it can "scan" its environment. Circling in a ring zone around the center when the correct distance of the platform to the wall is learned is considered "chaining". These non-spatial strategies dominate in the early learning phase. As the training progresses, mice develop spatially more precise and thus hippocampus-dependent search behavior. "Distracted search" is considered as transition between non-spatial and spatial strategies. Here, the animals search with preference for a relatively small pool area before they swim straightly to the platform.

In "directed search", the animal navigates mainly in the "goal corridor", a direct path between starting point and platform with a given width, still allowing for some uncertainty in the search. In "focal search", the mouse heads directly to the goal, searches closely to the platform before mounting it. The most direct path between start and goal is used during "straight swimming". These three swim patterns were summarized in the category "allocentric (other-centered) search" because here the animal uses the spatial arrangement of the experimental room, rather than its own current location, to find the hidden platform. Lastly, "perseverance" describes a persistent search in the former platform quadrant after moving the goal during the reversal part.

For the automated assignment of the swim paths to the defined categories, the parameters recorded with Sygnis Tracker software were used to derive descriptive criteria for the different search categories. The individual runs were classified using a decision tree built on the parameter space of all obtained data. When the run did not fall into any of the nine categories: (i) straight swimming, (ii) focal search, (iii) directed search, (iv) perseverance, (v) chaining, (vi) thigmotaxis, (vii) scanning, (viii) random search, (ix) distracted search—it was classified as unknown. Throughout our analysis, the rate of unknown strategies was < 8%.

Statistics and data analysis in behavioral tests

Results are shown as mean ± SEM. Statistical significance was determined using two-tailed unpaired Student's *t*-test, unless otherwise stated. To judge the performance of the animals over time in the T-maze, Poisson regression with autoregressive GEE (generalized estimating equation) (Ziegler & Vens, 2011) model was applied. In particular, for each genotype, it was tested whether the slope of the log best fit over days 1–10 differed significantly from zero. Similarly, a difference in the overall performances between the two genotypes was statistically tested by examining the interaction between the genotype and time variable, that is, to compare the slopes of the log best fits. Differences with $P < 0.05$ were considered statistically significant.

Significances were depicted as $*P < 0.05$, $**P < 0.01$, and $***P < 0.001$.

Expanded View for this article is available online.

Author contributions

JB-L planned and performed all behavioral experiments, morphological stainings, and analyzed these data. AK and BF performed affinity purifications and mass spectrometry analysis. VF generated and VF, AK, and BF validated TRPC antibodies. BS, RG, and YS performed electrophysiological analysis and fluorescence microscopy in cultured neurons under supervision of DB. JP and GK performed slice physiology. IM, HS, and RS gave conceptual input in behavioral and morphological studies. AL developed the algorithm for the pattern analysis. VNC, MB, and ADr performed electrophysiological recordings *in vivo*. PW participated in the generation of mouse lines and mouse breeding. ADi provided a mouse line. The manuscript was initially written by JB and MF. DB, RS, JP, GK, BF, AK, and VF complemented the manuscript and made critical revision. MF and DB conceived, designed, and supervised the study.

Conflict of interest

The authors declare that they have no conflict of interest.

References

Aggleton JP, Hunt PR, Rawlins JN (1986) The effects of hippocampal lesions upon spatial and non-spatial tests of working memory. *Behav Brain Res* 19: 133–146

Arns M, Sauvage M, Steckler T (1999) Excitotoxic hippocampal lesions disrupt allocentric spatial learning in mice: effects of strain and task demands. *Behav Brain Res* 106: 151–164

Ayala JE, Chen Y, Banko JL, Sheffler DJ, Williams R, Telk AN, Watson NL, Xiang Z, Zhang Y, Jones PJ, Lindsley CW, Olive MF, Conn PJ (2009) mGluR5 positive allosteric modulators facilitate both hippocampal LTP and LTD and enhance spatial learning. *Neuropsychopharmacology* 34: 2057–2071

Balschun D, Manahan-Vaughan D, Wagner T, Behnisch T, Reymann KG, Wetzel W (1999) A specific role for group I mGluRs in hippocampal LTP and hippocampus-dependent spatial learning. *Learn Mem* 6: 138–152

Bannerman DM, Good MA, Butcher SP, Ramsay M, Morris RG (1995) Distinct components of spatial learning revealed by prior training and NMDA receptor blockade. *Nature* 378: 182–186

Bannerman DM, Niewoehner B, Lyon L, Romberg C, Schmitt WB, Taylor A, Sanderson DJ, Cottam J, Sprengel R, Seeburg PH, Kohr G, Rawlins JN (2008) NMDA receptor subunit NR2A is required for rapidly acquired spatial

working memory but not incremental spatial reference memory. *J Neurosci* 28: 3623–3630

Bannerman DM, Bus T, Taylor A, Sanderson DJ, Schwarz I, Jensen V, Hvalby O, Rawlins JN, Seeburg PH, Sprengel R (2012) Dissecting spatial knowledge from spatial choice by hippocampal NMDA receptor deletion. *Nat Neurosci* 15: 1153–1159

Bannerman DM, Sprengel R, Sanderson DJ, McHugh SB, Rawlins JN, Monyer H, Seeburg PH (2014) Hippocampal synaptic plasticity, spatial memory and anxiety. *Nat Rev Neurosci* 15: 181–192

Bekkers JM, Stevens CF (1991) Excitatory and inhibitory autaptic currents in isolated hippocampal neurons maintained in cell culture. *Proc Natl Acad Sci USA* 88: 7834–7838

Bildl W, Haupt A, Muller CS, Biniossek ML, Thumfart JO, Huber B, Fakler B, Schulte U (2012) Extending the dynamic range of label-free mass spectrometric quantification of affinity purifications. *Mol Cell Proteomics* 11: M111.007955

Blair NT, Kaczmarek JS, Clapham DE (2009) Intracellular calcium strongly potentiates agonist-activated TRPC5 channels. *J Gen Physiol* 133: 525–546

Brigman JL, Wright T, Talani G, Prasad-Mulcare S, Jinde S, Seabold GK, Mathur P, Davis MI, Bock R, Gustin RM, Colbran RJ, Alvarez VA, Nakazawa K, Delpire E, Lovinger DM, Holmes A (2010) Loss of GluN2B-containing NMDA receptors in CA1 hippocampus and cortex impairs long-term depression, reduces dendritic spine density, and disrupts learning. *J Neurosci* 30: 4590–4600

Broadbent NJ, Squire LR, Clark RE (2004) Spatial memory, recognition memory, and the hippocampus. *Proc Natl Acad Sci USA* 101: 14515–14520

Chrobak JJ, Buzsaki G (1998) Gamma oscillations in the entorhinal cortex of the freely behaving rat. *J Neurosci* 18: 388–398

Collins SM, Surette M, Bercik P (2012) The interplay between the intestinal microbiota and the brain. *Nat Rev Microbiol* 10: 735–742

Davare MA, Fortin DA, Saneyoshi T, Nygaard S, Kaech S, Banker G, Soderling TR, Wayman GA (2009) Transient receptor potential canonical 5 channels activate Ca²⁺/calmodulin kinase Igamma to promote axon formation in hippocampal neurons. *J Neurosci* 29: 9794–9808

Deacon RM, Bannerman DM, Kirby BP, Croucher A, Rawlins JN (2002) Effects of cytotoxic hippocampal lesions in mice on a cognitive test battery. *Behav Brain Res* 133: 57–68

Dietrich A, Kalwa H, Storch U, Mederos y Schnitzler M, Salanova B, Pinkenburg O, Dubrovska G, Essin K, Gollasch M, Birnbaumer L, Gudermann T (2007) Pressure-induced and store-operated cation influx in vascular smooth muscle cells is independent of TRPC1. *Pflugers Arch* 455: 465–477

Dittman JS, Regehr WG (1998) Calcium dependence and recovery kinetics of presynaptic depression at the climbing fiber to Purkinje cell synapse. *J Neurosci* 18: 6147–6162

Du J, Creson TK, Wu LJ, Ren M, Gray NA, Falke C, Wei Y, Wang Y, Blumenthal R, Machado-Vieira R, Yuan P, Chen G, Zhuo M, Manji HK (2008) The role of hippocampal GluR1 and GluR2 receptors in manic-like behavior. *J Neurosci* 28: 68–79

Du J, Ma X, Shen B, Huang Y, Birnbaumer L, Yao X (2014) TRPV4, TRPC1, and TRPP2 assemble to form a flow-sensitive heteromeric channel. *FASEB J* 28: 4677–4685

Faber ES, Sedlak P, Vidovic M, Sah P (2006) Synaptic activation of transient receptor potential channels by metabotropic glutamate receptors in the lateral amygdala. *Neuroscience* 137: 781–794

Filali M, Lalonde R (2016) Neurobehavioral anomalies in the Pitx3/ak murine model of Parkinson's disease and MPTP. *Behav Genet* 46: 228–241

Fowler MA, Sidiropoulou K, Ozkan ED, Phillips CW, Cooper DC (2007) Corticolimbic expression of TRPC4 and TRPC5 channels in the rodent brain. *PLoS ONE* 2: e573

Freichel M, Suh SH, Pfeifer A, Schweig U, Trost C, Weissgerber P, Biel M, Philipp S, Freise D, Droogmans G, Hofmann F, Flockerzi V, Nilius B (2001) Lack of an endothelial store-operated Ca²⁺ current impairs agonist-dependent vasorelaxation in TRP4⁻/⁻ mice. *Nat Cell Biol* 3: 121–127

Freichel M, Vennekens R, Olausson J, Stolz S, Philipp SE, Weissgerber P, Flockerzi V (2005) Functional role of TRPC proteins in native systems: implications from knockout and knock-down studies. *J Physiol* 567: 59–66

Fuchs EC, Zivkovic AR, Cunningham MO, Middleton S, Lebeau FE, Bannerman DM, Rozov A, Whittington MA, Traub RD, Rawlins JN, Monyer H (2007) Recruitment of parvalbumin-positive interneurons determines hippocampal function and associated behavior. *Neuron* 53: 591–604

Garthe A, Behr J, Kempermann G (2009) Adult-generated hippocampal neurons allow the flexible use of spatially precise learning strategies. *PLoS ONE* 4: e5464

Goel M, Sinkins WG, Schilling WP (2002) Selective association of TRPC channel subunits in rat brain synaptosomes. *J Biol Chem* 277: 48303–48310

Greka A, Navarro B, Oancea E, Duggan A, Clapham DE (2003) TRPC5 is a regulator of hippocampal neurite length and growth cone morphology. *Nat Neurosci* 6: 837–845

Gross SA, Guzman GA, Wissenbach U, Philipp SE, Zhu MX, Bruns D, Cavalie A (2009) TRPC5 is a Ca²⁺-activated channel functionally coupled to Ca²⁺-selective ion channels. *J Biol Chem* 284: 34423–34432

Guzman RE, Schwarz YN, Rettig J, Bruns D (2010) SNARE force synchronizes synaptic vesicle fusion and controls the kinetics of quantal synaptic transmission. *J Neurosci* 30: 10272–10281

Hartmann J, Dragicevic E, Adelsberger H, Henning HA, Sumser M, Abramowitz J, Blum R, Dietrich A, Freichel M, Flockerzi V, Birnbaumer L, Konnerth A (2008) TRPC3 channels are required for synaptic transmission and motor coordination. *Neuron* 59: 392–398

Hofmann T, Schaefer M, Schultz G, Gudermann T (2002) Subunit composition of mammalian transient receptor potential channels in living cells. *Proc Natl Acad Sci USA* 99: 7461–7466

Hong C, Seo H, Kwak M, Jeon J, Jang J, Jeong EM, Myeong J, Hwang YJ, Ha K, Kang MJ, Lee KP, Yi EC, Kim IG, Jeon JH, Ryu H, So I (2015) Increased TRPC5 glutathionylation contributes to striatal neuron loss in Huntington's disease. *Brain* 138: 3030–3047

Hughes RN (2004) The value of spontaneous alternation behavior (SAB) as a test of retention in pharmacological investigations of memory. *Neurosci Biobehav Rev* 28: 497–505

Hui H, McHugh D, Hannan M, Zeng F, Xu SZ, Khan SU, Levenson R, Beech DJ, Weiss JL (2006) Calcium-sensing mechanism in TRPC5 channels contributing to retardation of neurite outgrowth. *J Physiol* 572: 165–172

Izquierdo I, Medina JH (1997) Memory formation: the sequence of biochemical events in the hippocampus and its connection to activity in other brain structures. *Neurobiol Learn Mem* 68: 285–316

Jang EH, Ahn SH, Lee YS, Lee HR, Kaang BK (2013) Effect of food deprivation on a delayed nonmatch-to-place T-maze task. *Exp Neurobiol* 22: 124–127

Jensen V, Kaiser KM, Borchardt T, Adelmann G, Rozov A, Burnashev N, Brix C, Frotscher M, Andersen P, Hvalby O, Sakmann B, Seeburg PH, Sprengel R (2003) A juvenile form of postsynaptic hippocampal long-term potentiation in mice deficient for the AMPA receptor subunit GluR-A. *J Physiol* 553: 843–856

Jeon JP, Roh SE, Wie J, Kim J, Kim H, Lee KP, Yang D, Jeon JH, Cho NH, Kim IG, Kang DE, Kim HJ, So I (2013) Activation of TRPC4beta by Galphai subunit increases Ca^{2+} selectivity and controls neurite morphogenesis in cultured hippocampal neuron. *Cell Calcium* 54: 307–319

Jiang S, Su J, Yao S, Zhang Y, Cao F, Wang F, Wang H, Li J, Xi S (2014) Fluoride and arsenic exposure impairs learning and memory and decreases mGluR5 expression in the hippocampus and cortex in rats. *PLoS ONE* 9: e96041

Kemp N, McQueen J, Faulkes S, Bashir ZI (2000) Different forms of LTD in the CA1 region of the hippocampus: role of age and stimulus protocol. *Eur J Neurosci* 12: 360–366

Kerchner GA, Nicoll RA (2008) Silent synapses and the emergence of a postsynaptic mechanism for LTP. *Nat Rev Neurosci* 9: 813–825

Kim SJ, Kim YS, Yuan JP, Petralia RS, Worley PF, Linden DJ (2003) Activation of the TRPC1 cation channel by metabotropic glutamate receptor mGluR1. *Nature* 426: 285–291

Kim JI, Lee HR, Sim SE, Baek J, Yu NK, Choi JH, Ko HG, Lee YS, Park SW, Kwak C, Ahn SJ, Choi SY, Kim H, Kim KH, Backx PH, Bradley CA, Kim E, Jang DJ, Lee K, Kim SJ *et al* (2011) PI3Kgamma is required for NMDA receptor-dependent long-term depression and behavioral flexibility. *Nat Neurosci* 14: 1447–1454

Kohr G, Jensen V, Koester HJ, Mihaljevic AL, Utvik JK, Kvello A, Ottersen OP, Seeburg PH, Sprengel R, Hvalby O (2003) Intracellular domains of NMDA receptor subtypes are determinants for long-term potentiation induction. *J Neurosci* 23: 10791–10799

Korotkova T, Fuchs EC, Ponomarenko A, von Engelhardt J, Monyer H (2010) NMDA receptor ablation on parvalbumin-positive interneurons impairs hippocampal synchrony, spatial representations, and working memory. *Neuron* 68: 557–569

Li Y, Jia YC, Cui K, Li N, Zheng ZY, Wang YZ, Yuan XB (2005) Essential role of TRPC channels in the guidance of nerve growth cones by brain-derived neurotrophic factor. *Nature* 434: 894–898

Li M, Chen C, Zhou Z, Xu S, Yu Z (2012) A TRPC1-mediated increase in store-operated Ca^{2+} entry is required for the proliferation of adult hippocampal neural progenitor cells. *Cell Calcium* 51: 486–496

Lipstein N, Sakaba T, Cooper BH, Lin KH, Strenzke N, Ashery U, Rhee JS, Taschenberger H, Neher E, Brose N (2013) Dynamic control of synaptic vesicle replenishment and short-term plasticity by Ca(2+)-calmodulin-Munc13-1 signaling. *Neuron* 79: 82–96

Logue SF, Paylor R, Wehner JM (1997) Hippocampal lesions cause learning deficits in inbred mice in the Morris water maze and conditioned-fear task. *Behav Neurosci* 111: 104–113

Ma X, Cheng KT, Wong CO, O'Neil RG, Birnbaumer L, Ambudkar IS, Yao X (2011) Heteromeric TRPV4-C1 channels contribute to store-operated Ca (2+) entry in vascular endothelial cells. *Cell Calcium* 50: 502–509

Malleret G, Hen R, Guillou JL, Segu L, Buhot MC (1999) 5-HT1B receptor knock-out mice exhibit increased exploratory activity and enhanced spatial memory performance in the Morris water maze. *J Neurosci* 19: 6157–6168

Montell C, Birnbaumer L, Flockerzi V (2002) The TRP channels, a remarkably functional family. *Cell* 108: 595–598

Morris RG, Garrud P, Rawlins JN, O'Keefe J (1982) Place navigation impaired in rats with hippocampal lesions. *Nature* 297: 681–683

Morris RG, Anderson E, Lynch GS, Baudry M (1986a) Selective impairment of learning and blockade of long-term potentiation by an N-methyl-D-aspartate receptor antagonist, AP5. *Nature* 319: 774–776

Morris RG, Hagan JJ, Rawlins JN (1986b) Allocentric spatial learning by hippocampectomised rats: a further test of the "spatial mapping" and "working memory" theories of hippocampal function. *Q J Exp Psychol B* 38: 365–395

Morris RG, Schenk F, Tweedie F, Jarrard LE (1990) Ibotenate lesions of hippocampus and/or subiculum: dissociating components of allocentric spatial learning. *Eur J Neurosci* 2: 1016–1028

Neves G, Cooke SF, Bliss TV (2008) Synaptic plasticity, memory and the hippocampus: a neural network approach to causality. *Nat Rev Neurosci* 9: 65–75

Nicholls RE, Alarcon JM, Malleret G, Carroll RC, Grody M, Vronskaya S, Kandel ER (2008) Transgenic mice lacking NMDAR-dependent LTD exhibit deficits in behavioral flexibility. *Neuron* 58: 104–117

Paxinos G, Franklin KBJ (2001) *The mouse brain in stereotaxic coordinates*. London, UK: Academic Press

Penley SC, Gaudet CM, Threlkeld SW (2013) Use of an eight-arm radial water maze to assess working and reference memory following neonatal brain injury. *J Vis Exp* 82: e50940

Pereira J, Wang XJ (2015) A tradeoff between accuracy and flexibility in a working memory circuit endowed with slow feedback mechanisms. *Cereb Cortex* 25: 3586–3601

Phelan KD, Mock MM, Kretz O, Shwe UT, Kozhemyakin M, Greenfield LJ, Dietrich A, Birnbaumer L, Freichel M, Flockerzi V, Zheng F (2012) Heteromeric canonical transient receptor potential 1 and 4 channels play a critical role in epileptiform burst firing and seizure-induced neurodegeneration. *Mol Pharmacol* 81: 384–392

Phelan KD, Shwe UT, Abramowitz J, Wu H, Rhee SW, Howell MD, Gottschall PE, Freichel M, Flockerzi V, Birnbaumer L, Zheng F (2013) Canonical transient receptor channel 5 (TRPC5) and TRPC1/4 contribute to seizure and excitotoxicity by distinct cellular mechanisms. *Mol Pharmacol* 83: 429–438

Reisel D, Bannerman DM, Schmitt WB, Deacon RM, Flint J, Borchardt T, Seeburg PH, Rawlins JN (2002) Spatial memory dissociations in mice lacking GluR1. *Nat Neurosci* 5: 868–873

Riccio A, Li Y, Moon J, Kim KS, Smith KS, Rudolph U, Gapon S, Yao GL, Tsvetkov E, Rodig SJ, Van't Veer A, Meloni EG, Carlezon WA Jr, Bolshakov VY, Clapham DE (2009) Essential role for TRPC5 in amygdala function and fear-related behavior. *Cell* 137: 761–772

Riccio A, Li Y, Tsvetkov E, Gapon S, Yao GL, Smith KS, Engin E, Rudolph U, Bolshakov VY, Clapham DE (2014) Decreased anxiety-like behavior and Galphaq/11-dependent responses in the amygdala of mice lacking TRPC4 channels. *J Neurosci* 34: 3653–3667

Riedel G, Reymann KG (1996) Metabotropic glutamate receptors in hippocampal long-term potentiation and learning and memory. *Acta Physiol Scand* 157: 1–19

Sailer CA, Hu H, Kaufmann WA, Trieb M, Schwarzer C, Storm JF, Knaus HG (2002) Regional differences in distribution and functional expression of small-conductance Ca^{2+}-activated K$^+$ channels in rat brain. *J Neurosci* 22: 9698–9707

Sanderson DJ, Good MA, Skelton K, Sprengel R, Seeburg PH, Rawlins JN, Bannerman DM (2009) Enhanced long-term and impaired short-term spatial memory in GluA1 AMPA receptor subunit knockout mice: evidence for a dual-process memory model. *Learn Mem* 16: 379–386

Scheffer-Teixeira R, Belchior H, Caixeta FV, Souza BC, Ribeiro S, Tort AB (2012) Theta phase modulates multiple layer-specific oscillations in the CA1 region. *Cereb Cortex* 22: 2404–2414

Scheffzuk C, Kukushka VI, Vyssotski AL, Draguhn A, Tort AB, Brankack J (2013) Global slowing of network oscillations in mouse neocortex by diazepam. *Neuropharmacology* 65: 123–133

Schmitt WB, Sprengel R, Mack V, Draft RW, Seeburg PH, Deacon RM, Rawlins JN, Bannerman DM (2005) Restoration of spatial working memory by genetic rescue of GluR-A-deficient mice. *Nat Neurosci* 8: 270–272

Schoch S, Deak F, Konigstorfer A, Mozhayeva M, Sara Y, Sudhof TC, Kavalali ET (2001) SNARE function analyzed in synaptobrevin/VAMP knockout mice. *Science* 294: 1117–1122

Schwenk J, Baehrens D, Haupt A, Bildl W, Boudkkazi S, Roeper J, Fakler B, Schulte U (2014) Regional diversity and developmental dynamics of the AMPA-receptor proteome in the mammalian brain. *Neuron* 84: 41–54

Schwenk J, Perez-Garci E, Schneider A, Kollewe A, Gauthier-Kemper A, Fritzius T, Raveh A, Dinamarca MC, Hanuschkin A, Bildl W, Klingauf J, Gassmann M, Schulte U, Bettler B, Fakler B (2016) Modular composition and dynamics of native GABAB receptors identified by high-resolution proteomics. *Nat Neurosci* 19: 233–242

Shen H, Pan J, Pan L, Zhang N (2013) TRPC6 inhibited NMDA current in cultured hippocampal neurons. *Neuromolecular Med* 15: 389–395

Steigerwald F, Schulz TW, Schenker LT, Kennedy MB, Seeburg PH, Kohr G (2000) C-Terminal truncation of NR2A subunits impairs synaptic but not extrasynaptic localization of NMDA receptors. *J Neurosci* 20: 4573–4581

Stevens CF, Wesseling JF (1998) Activity-dependent modulation of the rate at which synaptic vesicles become available to undergo exocytosis. *Neuron* 21: 415–424

Storch U, Forst AL, Philipp M, Gudermann T, Mederos y Schnitzler M (2012) Transient receptor potential channel 1 (TRPC1) reduces calcium permeability in heteromeric channel complexes. *J Biol Chem* 287: 3530–3540

Stroh O, Freichel M, Kretz O, Birnbaumer L, Hartmann J, Egger V (2012) NMDA receptor-dependent synaptic activation of TRPC channels in olfactory bulb granule cells. *J Neurosci* 32: 5737–5746

Strübing C, Krapivinsky G, Krapivinsky L, Clapham DE (2001) TRPC1 and TRPC5 form a novel cation channel in mammalian brain. *Neuron* 29: 645–655

Strübing C, Krapivinsky G, Krapivinsky L, Clapham DE (2003) Formation of novel TRPC channels by complex subunit interactions in embryonic brain. *J Biol Chem* 278: 39014–39019

Tort AB, Kramer MA, Thorn C, Gibson DJ, Kubota Y, Graybiel AM, Kopell NJ (2008) Dynamic cross-frequency couplings of local field potential oscillations in rat striatum and hippocampus during performance of a T-maze task. *Proc Natl Acad Sci USA* 105: 20517–20522

Tsien JZ, Chen DF, Gerber D, Tom C, Mercer EH, Anderson DJ, Mayford M, Kandel ER, Tonegawa S (1996a) Subregion- and cell type-restricted gene knockout in mouse brain. *Cell* 87: 1317–1326

Tsien JZ, Huerta PT, Tonegawa S (1996b) The essential role of hippocampal CA1 NMDA receptor-dependent synaptic plasticity in spatial memory. *Cell* 87: 1327–1338

Wang LY, Kaczmarek LK (1998) High-frequency firing helps replenish the readily releasable pool of synaptic vesicles. *Nature* 394: 384–388

Wenk GL (2001) Assessment of spatial memory using the T maze. *Curr Protoc Neurosci* Chapter 8: Unit 8 5B

Wu LJ, Sweet TB, Clapham DE (2010) International Union of Basic and Clinical Pharmacology. LXXVI. Current progress in the mammalian TRP ion channel family. *Pharmacol Rev* 62: 381–404

Wulff P, Ponomarenko AA, Bartos M, Korotkova TM, Fuchs EC, Bahner F, Both M, Tort AB, Kopell NJ, Wisden W, Monyer H (2009) Hippocampal theta rhythm and its coupling with gamma oscillations require fast inhibition onto parvalbumin-positive interneurons. *Proc Natl Acad Sci USA* 106: 3561–3566

Xing R, Zhang Y, Xu H, Luo X, Chang RC, Liu J, Yang X (2016) Spatial memory impairment by TRPC1 depletion is ameliorated by environmental enrichment. *Oncotarget* 7: 27855–27873

Xue T, Do MT, Riccio A, Jiang Z, Hsieh J, Wang HC, Merbs SL, Welsbie DS, Yoshioka T, Weissgerber P, Stolz S, Flockerzi V, Freichel M, Simon MI, Clapham DE, Yau KW (2011) Melanopsin signalling in mammalian iris and retina. *Nature* 479: 67–73

Zamanillo D, Sprengel R, Hvalby O, Jensen V, Burnashev N, Rozov A, Kaiser KM, Koster HJ, Borchardt T, Worley P, Lubke J, Frotscher M, Kelly PH, Sommer B, Andersen P, Seeburg PH, Sakmann B (1999) Importance of AMPA receptors for hippocampal synaptic plasticity but not for spatial learning. *Science* 284: 1805–1811

Zhang S, Wang W, Li J, Cheng K, Zhou J, Zhu D, Yang D, Liang Z, Fang L, Liao L, Xie P (2016) Behavioral characterization of CD36 knockout mice with SHIRPA primary screen. *Behav Brain Res* 299: 90–96

Ziegler A, Vens M (2011) Generalized estimating equations. *Methods Inf Med* 49: 421–425